Solving hindered groundwater dynamics in restored tidal marshes by creek excavation and soil amendments : a model study

Reference:
Van Putte Niels, Meire Patrick, Seuntjens Piet, Joris Ingeborg, Verreydt Goedele, Hambsch Lorenz, Temmerman Stijn.- Solving hindered groundwater dynamics in restored tidal marshes by creek excavation and soil amendments : a model study
Ecological engineering: the journal of ecotechnology - ISSN 1872-6992 - 178(2022), 106583
Full text (Publisher's DOI): https://doi.org/10.1016/J.ECOLENG.2022.106583
To cite this reference: https://hdl.handle.net/10067/1866050151162165141

Solving hindered groundwater dynamics in restored tidal marshes by creek excavation and soil amendments: a model study

Niels Van Putte*[1], Patrick Meire[1], Piet Seuntjens[1,2,5], Ingeborg Joris[2,4], Goedele Verreydt[1,3], Lorenz Hambsch[2], Stijn Temmerman[1]

[1]Ecosphere, Department of Biology, University of Antwerp, Antwerp, Belgium
[2]VITO (Flemish institute for technological research), Mol, Belgium
[3]iFLUX, Niel, Belgium
[4]Department of Bioscience Engineering, University of Antwerp, Antwerp, Belgium
[5]Biomath, Department of Mathematical Modelling and Analysis, Ghent University, Ghent, Belgium

*corresponding author: niels.vanputte@uantwerpen.be

Keywords: groundwater modelling, solute transport, marsh restoration, creek excavation, soil amendments

Highlights:

- Historical soil compaction limits groundwater flow in restored tidal marshes
- Seepage volumes were found to be 6 times less in restored marsh with compact subsoil
- Creek excavation and soil amendments increase soil – groundwater interactions
- Groundwater modelling is a useful tool to optimize tidal marsh restoration design

Graphical abstract:

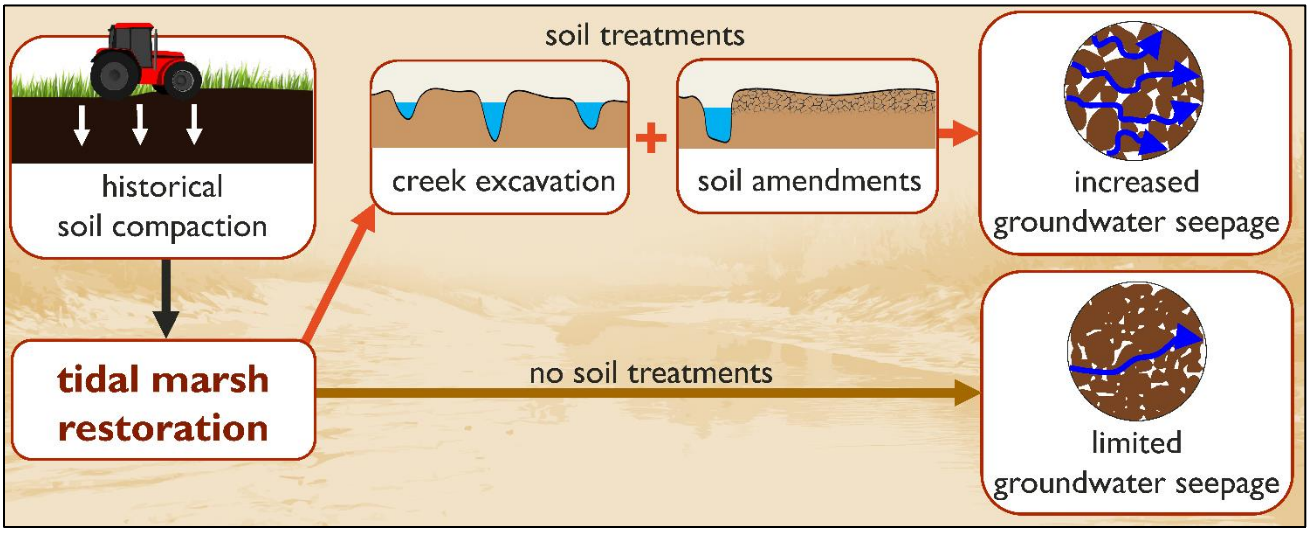

ABSTRACT

Groundwater fluxes in tidal marshes largely control key ecosystem functions and services, such as vegetation growth, soil carbon sequestration, and nutrient cycling. In tidal marshes restored on formerly embanked agricultural land, groundwater fluxes are often limited as compared to nearby natural marshes, as a result of historical agricultural soil compaction. To improve the functioning of restored tidal marshes, knowledge is needed on how much certain design options can optimize soil-groundwater interactions in future restoration projects. Based on measured data on soil properties and tidally induced groundwater dynamics, we calibrated and evaluated a 2D vertical model of a creek-marsh cross-section, accounting for both saturated and unsaturated groundwater flow and solute transport in a variably saturated groundwater flow model. We found that model simulations of common restoration practices such as soil amendments (increasing the depth of porous soil on top of the compact layer) and creek excavation (increasing the creek density) increase the soil aeration depth and time, the drainage depth and the solute flux, and decrease the residence time of solutes in the porewater. Our simulations indicate that increasing the depth to the compact layer from 20 cm to 40 cm, or increasing the creek density from 1 creek to 2 creeks along a 50 m marsh transect (while maintaining the total creek cross-sectional area), in both cases more than doubles the volume of water processed by the marsh soil. We discuss that this may stimulate nutrient cycling. As such, our study demonstrates that groundwater modelling can support the design of marsh restoration measures aiming to optimize groundwater fluxes and related ecosystem services.

1. INTRODUCTION

The flow of shallow groundwater is a key process in the ecohydrological functioning of tidal marsh ecosystems. When tidal marshes are inundated at high tide, part of the flooding water infiltrates into the marsh surface. At low tide, part of this water seeps out of the creek banks, lowering the groundwater level especially in the vicinity of tidal creeks (e.g. Chapman, 1938; Harvey et al., 1987). These tidally induced temporal and spatial variations in groundwater level control the soil aeration conditions (Li et al., 2005; Ursino et al., 2004), which further affect key ecosystem functions such as soil organic carbon storage or decomposition (Guimond et al., 2020) and vegetation zonation patterns (Wilson et al., 2015; Xie et al., 2020; Xin et al., 2013). Groundwater flow also regulates the cycling rate of nutrients in the marsh (Wang et al., 2011; Wilson and Gardner, 2006). As such, interactions between the groundwater and the soil are of high importance for the filtering capacity of tidal wetlands and their contribution to water quality improvement in the adjacent estuary. From the above, it is clear that groundwater dynamics are key for the delivery of regulating ecosystem services of tidal marsh ecosystems. Nevertheless, groundwater dynamics are rarely considered in the design of tidal marsh restoration schemes.

Along estuaries and coasts worldwide, there is an increasing demand for restoration of tidal marshes that have formerly been embanked, drained and converted to agricultural land. Marsh restoration is seen as a viable management strategy to counteract the loss of their ecosystem services due to large scale land reclamations in the past (Wolters et al., 2005). However, years after restoration, many restored tidal marshes still exhibit an impaired delivery of soil related ecosystem services compared to their natural counterparts. Their soil is often structurally different from the soil in natural tidal marshes (e.g. Burden et al., 2013; Craft et al., 2002; Van Putte et al., 2020). In natural tidal marshes, the soil consists of tidally deposited sediment, intermixed with plant debris and large void spaces, creating a macroporous soil. In the embanked areas, agricultural practices such as drainage of the soil and the use of heavy farming equipment often lead to mineralization of organic matter, compaction and consolidation of the soil, reducing its porosity and hydraulic conductivity. When a tidal marsh is restored on such an embanked land, this compact soil may act as an impermeable barrier for soil-water interactions (Crooks and Pye, 2000; Spencer et al., 2017; Van Putte et al., 2020). Groundwater level fluctuations and hence nutrient cycling are restricted to the layer of tidally deposited sediment that accumulates on top of the compact soil over time, whereas in natural marsh systems, groundwater and nutrient flow may occur over much deeper portions of the soil profile (Tempest et al., 2015; Van Putte et al., 2020). Given the above, there is an urgent need to counteract the restrictions of the compact soil and to optimize soil-groundwater interactions in future tidal marsh restoration projects.

Since the 1980’s, many efforts were made to simulate groundwater dynamics in natural tidal marshes. The complexity of these models increased over time (Marois and Stecher, 2020). Moffett et al. (2012) give an extended overview of the earliest models. These first models are restricted to simulating flow in the saturated zone (Harvey et al., 1987; Nuttle, 1988), while later developed models use the Richards’ equation to simulate both saturated and unsaturated flow (Ursino et al., 2004; Wilson and Gardner, 2006; Xin et al., 2009b). Several modelling studies consider a dual layered soil stratigraphy (Gardner, 2007; Xin et al., 2012) and some models also incorporate the effects of evapotranspiration (Hemond and Fifield, 1982; Ursino et al., 2004; Xin et al., 2017) and/or soil compressibility (Gardner and Wilson, 2006; Xin et al., 2009a). Only in a limited number of model studies, groundwater flow is coupled to solute transport (Chassagne et al., 2012; Wilson and Gardner, 2006). Recently, much attention is given to the presence of macropores, for instance created by burrowing invertebrate species, and their effect on groundwater flow in tidal marshes (Cao et al., 2012; Xin et al., 2009b; Xin et al., 2016; Xu et al., 2021). Until now, however, groundwater models have not yet been applied for modelling hindered groundwater flow and solute transport in restored tidal marshes with a historically compacted subsoil. Given the increasing number of marsh restoration projects in which this historical soil compaction hampers ecological development, improved scientific insights are needed on the impact of different restoration design options on groundwater flow and transport.

In this modelling study, we simulate the effect of several design options on the ecohydrological functioning of newly restored tidal marshes. Therefore, we apply a numerical groundwater model to a 2D marsh-creek cross section, using parameter values based on field measurements in a restored tidal marsh. In the marsh design scenarios, we vary **(a)** the creek density and (**b**) the depth of the compact layer. The rationale behind these design options is explained below.

- **(a)** Groundwater level fluctuations are typically strongest in the vicinity of tidal creeks. The majority of the seepage water originates from only a few meters from a tidal creek (Gardner, 2005a; Hughes et al., 1998; Xin et al., 2010). With this in mind, we hypothesize that initial excavation of a denser creek network in restored marshes will also increase the total seepage flux and increase the volume of the marsh soil that interacts with the groundwater. The excavation of an initial creek network prior to restoration is a common practice to enhance surface water drainage and vegetation establishment in restoration projects in which natural creek formation is inhibited or strongly slowed down by the relict compact soil (Liu et al., 2020; O'Brien and Zedler, 2006; Tovey et al., 2009; Vanlede et al., 2015).
- **(b)** As groundwater dynamics are inhibited by the compact soil layer, we hypothesize that the depth of this compact layer determines the depth of the soil profile over which soil-water interactions take place. To reverse the effect of historical agricultural soil compaction, organic soil amendments (e.g. ploughing and mixing wood chips with soil) prior to reflooding have been proposed as a management strategy to 'decompact" the soil and to obtain a soil structure comparable to that

found in natural tidal marshes (Callaway et al., 1997; Havens et al., 2002; Kadiri et al., 2011). Still, practical implementation of soil amendments in tidal marshes are rare (except Gibson et al., 1994; Ott et al., 2020; Zedler, 2000). For non-tidal wetland soils, however, several studies indicate the success of soil amendments in ameliorating soil structure (Fei et al., 2019; Scott et al., 2020; Wolf et al., 2019).

We determine the effect of these tidal marsh restoration design options on (i) groundwater drainage depth, (ii) soil saturation index (i.e. the proportion of the spring tide – neap tide cycle that a specific location in the marsh soil is saturated (Xin et al., 2010)) and (iii) the total seepage flux of both water and solutes. Lastly, we also estimate (iv) the residence time of the groundwater.

2. METHODS

2.1. Field data

2.1.1. Study site

The study site is situated in the restored marsh 'Lippenbroek', located along the freshwater tidal part of the Scheldt estuary in Belgium (51°05'06.8" N 4°10'19.3"E, Fig. 1b). The estuary has a semidiurnal tide with an average tidal range of approximately 6 m near the studied tidal marsh. This marsh experiences an inundation frequency (percentage of flooding high tides) of 56% at the study location. The marsh is restored on land that has been under agricultural practice since large scale land reclamation in the 13th century, by building of dikes and drainage of the original wetlands. It was restored to a tidal wetland in 2006 using the CRT (controlled reduced tide) principle described in Maris et al. (2007). Since the restoration, the mean elevation of the site increased with 2.35 cm year^{-1} on average due to accretion of tidal sediment (Oosterlee et al., 2017). On the study transect, 60 cm has been deposited on top of the compact agricultural soil. The vegetation consists of wetland plants, mainly reed (*Phragmites australis)* and cattail (*Typha latifolia*) in the lower elevated parts where the transect is located, and mainly willow trees (*Salix* sp.) and stinging nettle (*Urtica dioica*) in the higher elevated parts (Jacobs et al., 2009). Since the marsh restoration, a tidal channel network initially developed relatively rapidly, but the development slowed down after approximately 3 years, resulting in an estimated, approximate average distance of 27.4 m to the nearest tidal creek (Vandenbruwaene et al., 2012).

2.1.2. Transects and wells

A 22 m long cross-sectional transect from a tidal creek over the marsh platform was established in the field (Fig. 1c). On the transect, we placed one monitoring well in the creek to measure surface water level fluctuations and four monitoring wells in the marsh soil to study groundwater level fluctuations. These wells were placed at increasing distances form the creek (1 m, 4 m, 10 m and 22 m) as the groundwater level fluctuations were expected to decrease with an increasing distance from the creek (Van Putte et al., 2020). The monitoring wells were slotted over the entire below-ground part and placed up to a depth of 1.75 m below the soil surface. The pressure head in the wells was measured every minute with pressure transducers (Rugged Troll 100, In-Situ Inc.) and corrected for variations in atmospheric pressure. The surface topography of the transect and the absolute elevation of the wells was measured with a total station (Sokkia SET510k) and recorded in m relative to TAW (the Belgian ordnance datum). Approximately one month of groundwater level measurements (from the 24th of

January to the 21st of February 2019, i.e. two spring tide-neap tide cycles) was selected for our analyses.

2.1.3. Soil profiles and soil samples

Along the transect, the soil profile was described to determine the depth of the compacted agricultural soil relative to the soil surface. This was done with a gouge auger sampling the soil profile near every monitoring well along the transect, and allowing easy distinction between the compact layer and the loose sediment layer on top of it. In addition, undisturbed soil samples of 100 cm³ were taken at 2 – 7 cm depth (i.e., in the newly deposited sediment) and 100 – 105 cm depth (i.e., in the compact relict agricultural soil) in six replicates at each of the locations of the wells.

2.1.4. Soil hydraulic properties

Four out of six replicates of the soil samples were used to measure the dry bulk density (ρ_b) and the saturated hydraulic conductivity (K_s). These samples were fully saturated and K_s was measured using either the constant head method (Eijkelkamp Agrisearch Equipments, 2013) for high permeable soil samples and the falling head method for low permeable soils. For the latter, a burette inside a rubber stop cock was inserted in the sample holder. A positive pressure head was applied on the samples by filling the burette with water. While the water seeped through the samples, we noted the decline in pressure head over time. K_s was calculated using Darcy's law (Darcy, 1856) and exponential regression of the pressure head in function of time.

The remaining replicates were used to determine the SWRC (Soil Water Retention Curve) and were placed in a sandbox (Eijkelkamp Soil & Water, 2019). Suctions of 10 cm, 30 cm, 50 cm, 70 cm and 100 cm were applied. Samples were weighed after each pressure step after reaching equilibrium states to determine the volumetric water content (θ). The water retention at suctions of 340 cm, 1020 cm and 15300 cm was determined on a smaller subsample using ceramic plate extractors (Cresswell et al., 2008). The obtained volumetric soil moisture data in function of applied pressure were averaged over the two replicates. The SWRC was fitted with the retention/conductivity model of van Genuchten-Mualem (van Genuchten, 1980) with the RETC (RETention Curve) code formula described in Van Genuchten et al. (1991):

$$\theta(h) = \begin{cases} \theta_r + \dfrac{\theta_s - \theta_r}{[1 + |\alpha h|^n]^{1-1/n}} & h < 0 \\ \theta_s & h \geq 0 \end{cases} \qquad \text{EQ 1}$$

In EQ 1, $\theta(h)$ [-] is the volumetric soil water content in function of the pressure head h [L] expressed as the pressure exerted by a water column with height h, θ_r [-] is the residual water content and θ_s[-] is the saturated water content; n is an index for the pore size distribution and α is a shape factor that relates to the inverse of the air entry value.

2.2. model development

2.2.1. Domain properties

We set up a two-dimensional variably saturated groundwater model using the HYDRUS 2D/3D software (Senja et al., 2017). The model domain geometry is a creek-marsh cross section with an idealized topography that is approximating the measured average marsh platform elevation and the creek depth and width on the measuring transect (Fig. 1). The domain has a total length of 50 m. The domain bottom was chosen arbitrarily at 2 m below the marsh platform elevation. Deepest measured groundwater levels were never deeper than 0.5 m, and the creek depth was 1.5 m. No exchange with aquifers underneath was assumed due to the presence of the compact subsoil. The domain was divided into two layers: an upper layer of recently deposited sediment and a lower layer of compact relict agricultural soil. Based on field measurements, the soil layer transition was set at 0.60 m below the marsh platform elevation. For these two layers, the measured values for the soil hydraulic properties, averaged for the different locations on the transect, were attributed to the respective soil layer.

A finite element mesh (FEM) was generated for the model domain and consists of approximately 20000 nodes. Mesh refinements were made around the creek banks and the transition between soil layers where higher spatial differences in pressure head and water content were expected. Observation nodes were inserted in the mesh at the location and depth where monitoring wells were installed in the marsh (Fig. 1) to compare the measured and simulated groundwater levels.

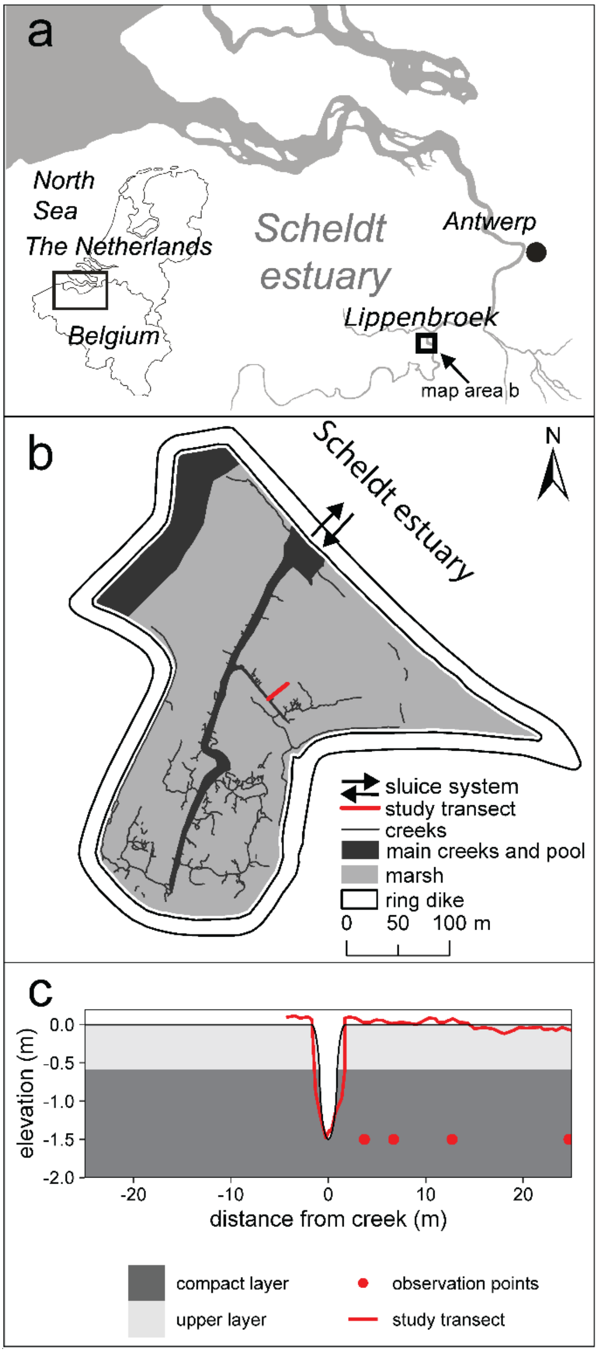

Fig. 1 a Situation of the study area within the Scheldt estuary b: Overview map of the study area (Lippenbroek) with indication of the study transect, c: model domain based on the measured transect elevation profile (in red).

2.2.2. Boundary and initial conditions

Fluctuations of the surface water level that were measured in the creek were imposed as a time variable pressure head boundary condition to the creek banks and the marsh platform. This boundary was allowed to develop into a seepage face where the nodal pressure became negative, i.e. at the border of the saturated flow field and the atmosphere. A no-flux boundary was applied at the sides and the bottom of the domain as no water was expected to enter or leave the domain via the bottom through the presence of the compact agricultural soil.

2.2.3. Governing equations

2.2.3.1. Water flow

To describe variably saturated water flow, the Richards' equation is solved (Richards, 1931). For a planar 2D vertical domain, this equation is given by EQ 2,

$$\frac{\partial \theta}{\partial t} = \frac{\partial}{\partial x}\left[K(h)\left(\frac{\partial h}{\partial x}+1\right)\right] + \frac{\partial}{\partial z}\left[K(h)\left(\frac{\partial h}{\partial z}+1\right)\right] \qquad \text{EQ 2}$$

in which θ [-] is the volumetric water content, h [L] is the pressure head and x [L] and z [L] are the spatial coordinates in the horizontal and vertical dimensions, t [T] is the time and $K(h)$ [LT^{-1}] is the hydraulic conductivity of the soil as a function of the pressure head, given by EQ 3 (van Genuchten, 1980).

$$K(h) = K_s S_e^l \left[1-\left(1-S_e^{\frac{n}{n-1}}\right)^{1-\frac{1}{n}}\right]^2 \qquad \text{EQ 3}$$

Here, n [-] is an index for the pore-size distribution, l [-] is the pore connectivity parameter taken as 0.5 (Mualem, 1976) and S_e [-] is the effective degree of saturation, which is given by EQ 4 (van Genuchten, 1980),

$$S_e = \frac{\theta - \theta_r}{\theta_s - \theta_r} \qquad \text{EQ 4}$$

where θ_r [-] is the residual water content and θ_s [-] is the saturated water content. Groundwater flow in tidal marsh sediments is known to occur mainly through macropores intersecting the sediment matrix (Harvey and Nuttle, 1995; Xiao et al., 2019; Xin et al., 2016). Therefore, our model was set up as a dual porosity model with a mobile (macropores) and an immobile (matrix) region. This model assumes that groundwater flow is restricted to the mobile region. The relative distribution of the matrix- and macropore space was estimated based on the results of micro-CT scans of soil cores from the same field site, described in Van Putte et al. (2020) in which macropores are defined as pores > 60 µm. The Richards equation (EQ 2) can be rewritten for both regions and a simple mass balance equation to describe a change in soil water moisture (EQ 5),

$$\frac{\partial \theta_m}{\partial t} = \frac{\partial}{\partial x}\left[K(h)\left(\frac{\partial h}{\partial x}+1\right)\right] + \frac{\partial}{\partial z}\left[K(h)\left(\frac{\partial h}{\partial z}+1\right)\right] - \Gamma_w \quad \text{and} \quad \frac{\partial \theta_{im}}{\partial t} = \Gamma_w \qquad \text{EQ 5}$$

with θ_m [-] and θ_{im} [-] being the volumetric soil moisture content in the mobile and the immobile region, respectively and Γ_w [T^{-1}] being the mass transfer from the mobile to the immobile region (Gerke and van Genuchten, 1993). This mass transfer rate is assumed to be proportional to the difference in effective saturation between the mobile and the immobile regions (EQ 6),

$$\Gamma_w = \frac{\partial \theta_{im}}{\partial t} = \omega[S_e^m - S_e^{im}] \qquad \text{EQ 6}$$

where S_e^m [-] and S_e^{im} [-] are the effective saturation of the mobile and the immobile region, respectively, and ω [T^{-1}]is a first order rate coefficient (Simunek et al., 2003). As ω depends on many unknown soil properties, the model was calibrated to find the best corresponding simulation for the measured pressure heads.

2.2.3.2. Residence time and solute transport

We estimated the residence time of the porewater in the marsh soil to determine the locations where water is replaced on a short time scale. For this purpose, the transport of a non-reactive solute was implemented in the model and we calculated for each location in the domain the half-life, i.e. the time it takes to remove half of the solute mass in that location. The initial tracer concentration in the pore water in the domain was set to 1 whereas the concentration in the flooding water was set to 0. As such, during the simulation, porewater seeps out of the creek banks and is replaced with flooding water. Since the residence time is essentially simulated as a 'tracer', this method takes into account dispersion and diffusion, in contrast to more traditional groundwater age determination methods such as particle tracking (Goode, 1996; Suckow, 2014; Turnadge and Smerdon, 2014; Wilson and Gardner, 2006).

For the dual porosity model, the solute flux equations for the mobile and immobile region are given by EQ 7 (advection dispersion equation) and EQ 8, respectively (van Genuchten and Wierenga, 1976).

$$\theta_m \frac{\partial c_m}{\partial t} = \frac{\partial}{\partial x}\left(\theta_m D_m \frac{\partial c_m}{\partial x}\right) - \frac{\partial q_x c_m}{\partial x} + \frac{\partial}{\partial z}\left(\theta_m D_m \frac{\partial c_m}{\partial z}\right) - \frac{\partial q_z c_m}{\partial z} - \Gamma_s \qquad \text{EQ 7}$$

$$\Gamma_s = \theta_{im} \frac{\partial c_{im}}{\partial t} = \omega_s (c - c_{im}) + \Gamma_w c^* \quad \text{With} \quad c^* = \begin{cases} c_m & \Gamma_w > 0 \\ c_{im} & \Gamma_w < 0 \end{cases} \qquad \text{EQ 8}$$

In these equations, c_m and c_{im} [ML^{-3}] are the concentrations of the solute in the mobile and immobile region, respectively. q_x and q_z [LT^{-1}]are the volumetric flux densities in the x and z dimension. Γ_s [MT^{-1}] is the solute exchange rate between the two regions and ω_s [T^{-1}] is the solute exchange rate coefficient. D_m [L] is the dispersion coefficient of the mobile region, which is defined as EQ 9,

$$D_m = \frac{\theta}{\theta_m} D \qquad \text{EQ 9}$$

where D [L] is the effective dispersion coefficient. Dispersion rates differ in the x and z direction. The dispersion for a vertical two-dimensional domain can be written as EQ 10 (Bear, 1972),

$$\begin{cases} \theta D_{xx} = D_L \frac{q_x^2}{|q|} + D_T \frac{q_z^2}{|q|} + \theta D_w \tau_w \\ \theta D_{zz} = D_L \frac{q_z^2}{|q|} + D_T \frac{q_z^2}{|q|} + \theta D_w \tau_w \\ \theta D_{xz} = (D_L - D_T) \frac{q_x q_z}{|q|} \end{cases} \qquad \text{EQ 10}$$

where D_L and D_T [L] are the longitudinal and transversal dispersivities, respectively, D_w [L] is the molecular diffusion coefficient and τ_w [-] is the tortuosity factor, which was estimated as EQ 11 by Millington and Quirk (1961).

$$\tau_w = \frac{\theta^{7/3}}{\theta_s^2} \qquad \text{EQ 11}$$

In our simulations, we assumed that the solute concentration in the immobile region is initially in equilibrium with the mobile region. Table 1 gives an overview of the values of the model input parameters and how they were defined.

Table 1: model input parameters

Soil layer	Upper layer	compact layer
ρ_b [g/cm³]	0.54 [a]	1.10 [a]
K_s [m/s]	$3.50 \cdot 10^{-5}$ [a,b]	$4.16 \cdot 10^{-8}$ [a]
$\theta_{s,m}$ [-]	0.05[a,c]	0.55 [a,c]
$\theta_{s,im}$ [-]	0.71[a,c]	0.01 [a,c]
$\theta_{r,m}$ [-]	0.00 [a,c]	0.00 [a,c]
$\theta_{r,im}$ [-]	0.09 [a,c]	0.01[a,c]
α [m^{-1}]	3.45 [a]	0.37 [a]
n [-]	1.19 [a]	1.18 [a]
ω [-]	$5.00 \cdot 10^{-3}$ [b]	$5.00 \cdot 10^{-3}$ [b]
D_L [m]	0.10 [d]	0.10 [d]
D_T [m]	0.01 [d]	0.01[d]
D_w [m²/s]	1.00·10-9 [e]	1.00·10-9 [e]
ω_s [s^{-1}]	$8.33 \cdot 10^{-7}$ [f]	$8.33 \cdot 10^{-7}$ [f]

[a] lab measurements on soil samples and parameter estimation with RETC
[b] model calibration
[c] based on micro-CT scans in Van Putte et al. (2020)
[d] based on Wilson and Gardner (2006)
[e] based on Holz et al. (2000)
[f] based on Jaynes and Horton (1998)

2.2.3.3. Drainage depth

We analyzed groundwater drainage depth on two time scales that are relevant in context of a tidal system, and we refer to these two time scales by introducing the terms "spring tide drainage depth" and "neap tide drainage depth". During about 10 days around the occurrence of spring tide, the marsh surface is flooded by most semi-diurnal high tides, and emerges during every semi-diurnal low tide (Fig. 2). The spring tide drainage depth is then defined as the average groundwater drainage depth below the soil surface in between tides that flood the marsh platform (i.e. the lowest groundwater level reached during the low water phase in between two high water phases that both inundate the marsh platform). The spring tide drainage depth relates to the zone which desaturates nearly every tide. The neap tide drainage depth is defined as the maximum drainage depth that occurred during the measured timespan. This drainage occurs during neap tide when the marsh platform is not inundated for several days (Fig. 2). Underneath the neap tide drainage depth, the soil remains always saturated. Drainage depths were calculated using the Tides package for R (Cox, 2017).

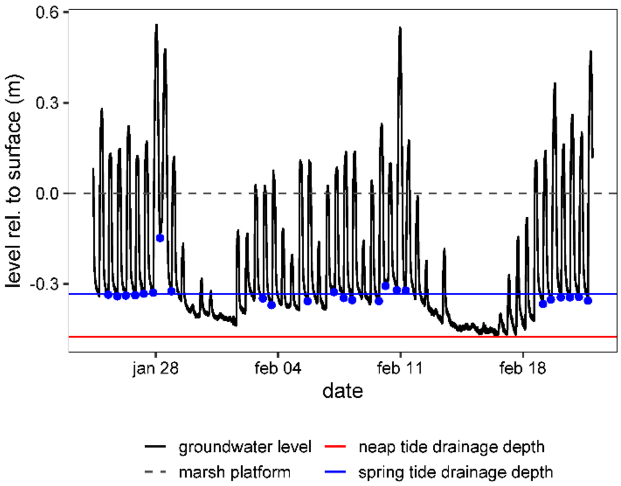

Fig. 2: Clarification of the newly introduced terms 'spring tide drainage depth' and 'neap tide drainage depth'. This figure represents the measured groundwater level at 1 m from the creek edge during two spring tide - neap tide cycles. The blue bullets indicate the drainage depth between consecutive flooding tides. The spring tide drainage depth is defined as the average of these values.

2.2.4. Sensitivity analysis

The model was tested for its sensitivity to values for the parameters K_s, α and the mass transfer coefficient ω (see Appendix). The saturated hydraulic conductivity K_s is the most important hydraulic parameter governing groundwater flow and seepage (Gardner, 2005b; Xin et al., 2012) and laboratory measurements revealed a wide variation on the data spanning multiple orders of magnitude (Fig. 3). The α parameter is a shape parameter of the SWRC and is roughly related to the inverse of the air entry value, the matric potential which corresponds to the beginning of desaturation (Van Genuchten et al., 1991). The ω value had to be calibrated because it could not be estimated form the measured hydraulic properties. A value of 0.05 resulted in the best model performance. The model performance was evaluated with the Nash-Sutcliffe model efficiency coefficient (EQ 12) (Nash and Sutcliffe, 1970) by comparing the simulated and measured pressure heads,

$$ME = 1 - \frac{\sum(OBS - SIM)^2}{\sum(OBS - MEAN)^2} \qquad \text{EQ 13}$$

where *ME* is the model efficiency coefficient, *OBS* are the observed pressure heads, *SIM* are the simulated pressure heads and *MEAN* is the mean of the observed pressure heads. Observed and simulated pressure heads during flooding of the marsh platform were not included in the evaluation since this would lead to overestimation of the model efficiency as the pressure head at the top boundary of the domain was set equal to the measured pressure head during inundation.

2.3. Scenario analyses

In total, we ran 25 different scenarios in which the depth (relative to the soil surface) of the compact layer and the number of creeks in the domain were varied. The depth of the compact layer was varied as 20 cm, 40 cm, 60 cm, 80 cm and 100 cm below the soil surface. A transition depth of 60 cm is the reference situation. A scenario with a deeper or less deep soil transition can represent either a difference in sedimentation rate of the marsh, or the depth to which soil amendments (e.g. tillage with addition of organic matter to increase soil porosity) are applied in a newly restored tidal marsh.

Model domains with 1, 2, 3, 4 and 5 creeks along the 50 m long transect were considered. As a result, the distance between the creeks varies from 50 m (1 creek in domain) to 10 m (5 creeks in domain). These distances are within the range of the average distance to the nearest tidal creek generally observed in tidal marshes (Chirol et al., 2018). When increasing the creek density, the creek width to depth ratio of all the creeks in the domain was conserved. This was done to approximate realistic scenarios, for which excavating of the creeks would result in creek dimensions that are expected to be close to morphodynamic equilibrium. At equilibrium, the total cross sectional area of creeks in a tidal marsh is proportional to the tidal prism, i.e. the total flood and ebb water volumes flooding onto and draining from the surrounding marsh platform surface area (D'Alpaos et al., 2010; Lawrence et al., 2004; Vandenbruwaene et al., 2013). Following this reasoning, in the different scenarios with increasing number of creeks over our cross-section, we made sure that total creek cross-sectional area remained constant, as tidal prism is not changing in between the different scenarios. Where the statistical significance of differences between the outcome of different scenarios was tested, we used a two-way ANOVA.

3. RESULTS

3.1. Field data and model input

3.1.1. Measured soil properties

An analysis of the soil properties reveals the distinct characteristics of the relict compact soil (lower layer) and the newly deposited sediment (upper layer). The bulk density in the lower layer is more than twice the bulk density in the upper layer (Fig. 3a). This difference is also reflected in the K_s values (Fig. 3b).

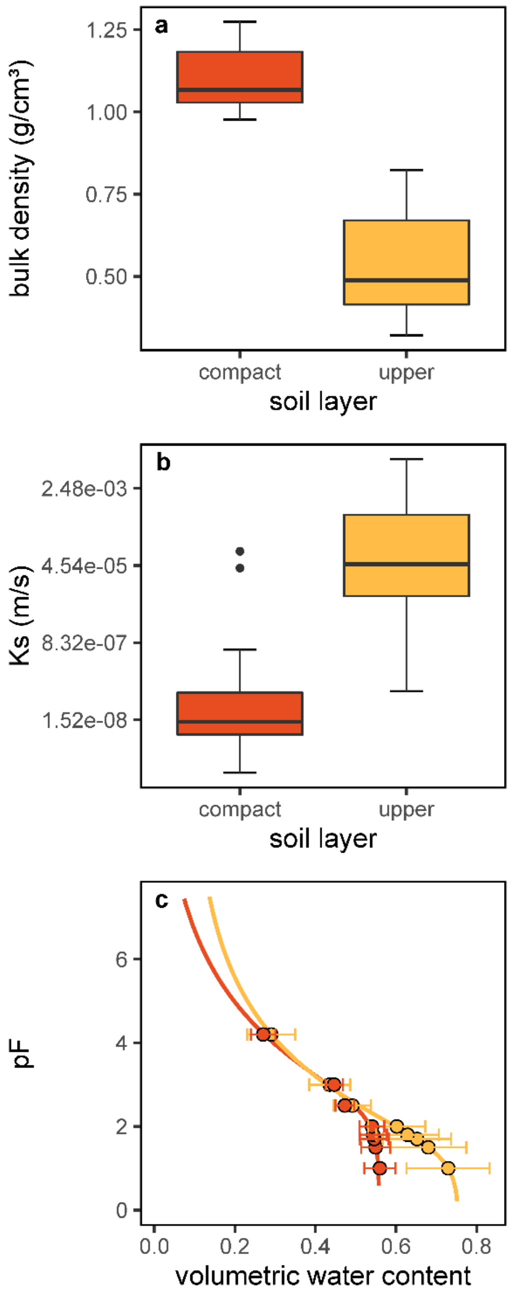

Fig. 3: soil hydraulic properties for the compact soil layer (orange) and the layer of newly deposited sediment (yellow). (a): boxplot of the bulk density (n=16) (b) boxplot of the saturated hydraulic conductivity (n=16) (note the logarithmic y-axis), (c): soil water retention curves. bullets indicate the measured water contents to the corresponding applied

suction and error bars represent the standard deviation on these values (n=8). Lines depict the regression curves using the van Genuchten – Mualem model (van Genuchten, 1980)

The hydraulic conductivity of the upper layer shows values ranging over several orders of magnitude, denoting a large spatial heterogeneity of soil physical properties and the presence of macropores. The hydraulic conductivity of the lower layer is on average 1476 times lower and less variable than in the upper layer (Fig. 3b). Fig. 3c shows the soil water retention curve for both soil layers. The upper soil layer has a higher porosity (Table 1). In the low pressure range (10 – 100 cm), the soil water content decreases more with an increasing suction in the upper layer compared to the lower layer, indicating the presence of larger pores in the upper layer. At higher suctions, the soil water retention curves for both layers converge.

3.1.2. Measured subsurface hydrology

The subsurface hydrology measured at the transect follows a distinctive pattern. During flooding of the marsh platform, the water level in the wells approximates the surface water level (Fig. 4). In all wells, but especially in the well at 4 m from the creek, a time lag is observed. When the tide recedes towards low tide, the groundwater level declines until the next flooding high tide. This decline is more profound close to the creek and attenuated further away from the creek.

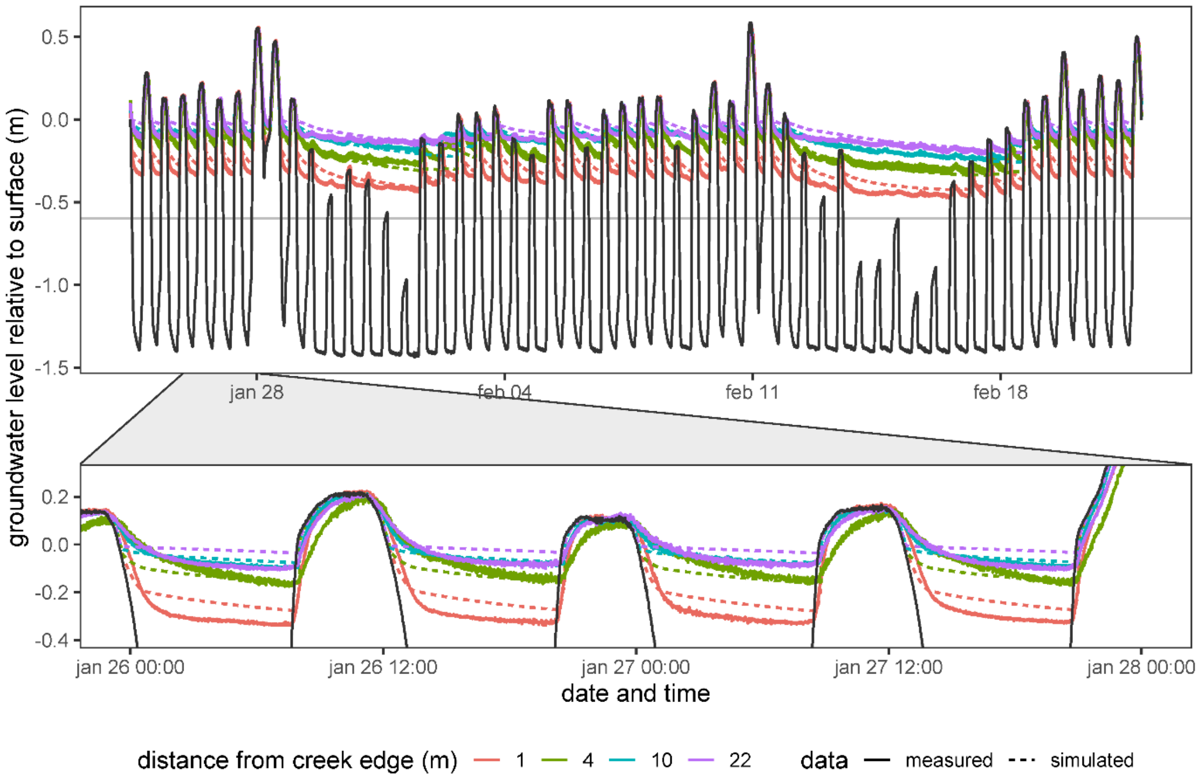

Fig. 4: Comparison of the measured and simulated groundwater level fluctuations on a transect perpendicular to a tidal creek in the restored marsh covering two spring tide - neap tide cycles in the winter of 2019. The solid black line represents the creek surface water level that was used as a time variable boundary condition in the model. The grey horizontal line indicates the approximate depth of the transition between the tidally deposited sediment and the underlying compact soil.

During neap tides, the groundwater level in the marsh soil declines further. Tides that only flood the creeks but not the marsh platform affect the groundwater level only in the close vicinity of the tidal creek. The groundwater level never falls below the transition between the newly deposited sediment and the compact soil, which remains always saturated.

3.2. Model performance

The model was run with the parameters indicated in Table 1. The model input parameters Ks, α and ω were calibrated to obtain the best simulated pressure heads. For these parameters, a sensitivity analysis was performed, which is summarized in the Appendix. The drainage depth was simulated with good accuracy (ME > 0.55) up till 10 m from the creek (Table 2).

Table 2: Nash-Sutcliffe model efficiency coefficient for simulated and measured pressure heads along the transect

Distance from creek edge	ME coefficient
1 m	0.57
4 m	0.68
10 m	0.66
22 m	-0.14

At 1 m from the creek, the model underestimated the spring tide drainage depth, which may be because of the steeper creek edge on the field transect vs. the modeled transect (Fig. 1). Our model always underestimated the drainage depth at 22 m from the creek. The latter may be because further away from the transect creek, other (smaller) creeks may also influence the local groundwater level in the field, while this is not represented in the model. Because in the scenario analysis we focus on scenarios with smaller distances between creeks, we decided to calibrate the unknown model parameters for best model performance on the results up to 10 m from the creek.

3.3. Impact of the compact layer on subsurface hydrology

We quantify the effect of the presence of the compact layer by making a comparison between the base scenario (compact layer at 60 cm depth) and a scenario without a compact layer (i.e. the entire soil profile consists of tidally deposited sediment). For the latter scenario, the lower layer was attributed the same hydraulic properties as the upper layer.

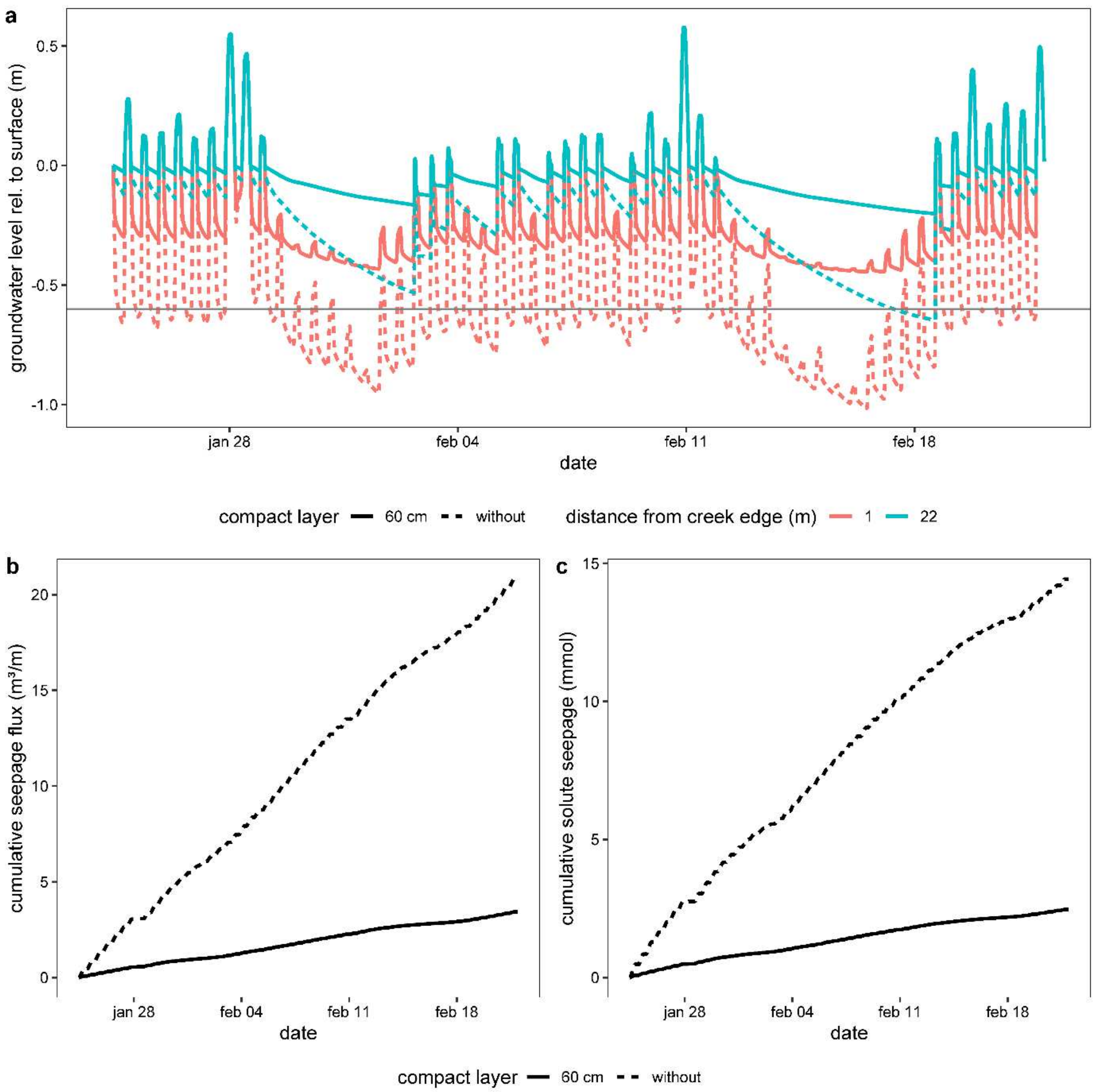

Fig. 5: comparison of a simulation in the absence of a compact layer and with a compact layer at a depth of 0.60 m. (a) groundwater level fluctuations during 2 spring tide – neap tide cycles near the creek and in the marsh interior. The grey horizontal line indicates the depth of the compact layer if present. (b) cumulative seepage flux per meter creek length. (c) cumulative solute seepage flux per meter creek length.

In between tides that flood the marsh platform, the spring tide drainage depth at 1 m from the creek is 0.28 m in the base scenario and 0.45 m in the scenario without a compact layer. In the marsh interior at 22 m from the creek, the difference in the spring tide drainage depth between the base scenario and the scenario without a compact layer is smaller (Fig. 5). Here, the effect of the compact layer is more pronounced in the neap tide drainage depth (0.04 m vs. 0.15 m). From Fig. 5a, it is apparent that in the marsh interior, the drainage depth depends mainly on the elapsed time since the last inundation of the marsh platform. Fig. 5b represents the cumulative seepage flux over the time. This is the total volume of water that passed through the marsh soil and seeped out of the creek banks during the simulated time. Without a compact soil layer, 6.06 times more water passes through the marsh soil compared to the current situation. The cumulative solute seepage flux (Fig. 5c), shows a similar pattern. The solute mass removed from the domain after two spring tide – neap tide cycles is 5.84 times higher without the presence of the compact layer. Especially in the run without the compact layer, the solute seepage rate slightly decreases near the end of the simulation. This indicates the start of depletion of solute in the zone near the creek.

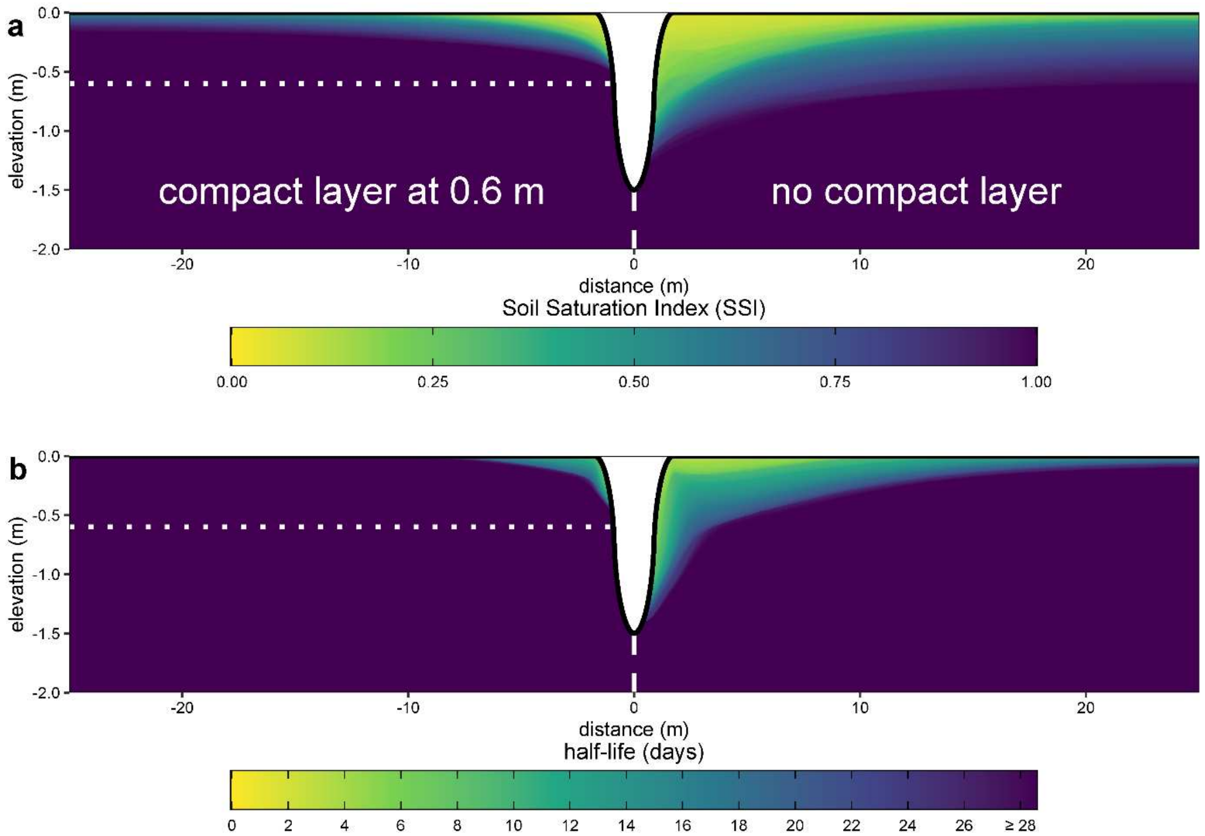

Fig.6: (a) Spatial distribution of the soil saturation index (SSI) for the simulation in the absence of a compact layer (right) and the simulation with a compact layer at 0.60 m (left). A value of 1 indicates that the soil at that location is saturated for 100% of the time. Saturated soil is defined as soil where $\theta \geq \theta_s - 0.01$. (b) spatial distribution of the solute half-life (i.e. the time it takes to remove half of the solute mass at a given location). A half-life of > 28 days means that no solute was removed in that location of the domain during the simulated timespan (2 spring tide – neap tide cycles). The dotted horizontal line represents the transition between the compact soil and the tidally deposited sediment.

The presence of the compact layer strongly affects the spatial distribution of the SSI (soil saturation index). The proportion of the domain in which the soil is unsaturated for at least half of a spring tide – neap tide cycle is 4.70 times higher without the presence of a compact layer compared to the base situation. In this base situation, the variably saturated zone (i.e. zone at least unsaturated for some of the time), is limited to only 0.38 m below the soil surface near the creek (at 1 m) and 0.15 m in the marsh interior (at 22 m from the creek edge, Fig.6a). In the simulation without a compact layer, this zone extends to a depth of 1.06 m near the creek and 0.60 m in the marsh interior.

The effect of the compact layer is also clearly present in the retention times of a non-reactive solute in the domain. Fig.6b shows the half-life (time it takes to remove half of the mass of the solute) for the domain. In the base simulation, the soil further away than ca. 7 m from the creek edge never loses half of its solute mass over the simulated 28-days period. Here, solute is only removed in the vicinity of the creeks. In the scenario without a compact layer, solute is partly removed up to a depth of 0.09 m, even in the marsh interior (22 m from the creek edge).

3.4. Scenario analyses for tidal marsh restoration design options

Model scenarios were run to simulate (i) creek excavation and (ii) soil amendments as possible restoration design options to optimize groundwater dynamics in newly restored tidal marshes. Therefore, 25 different model domains were made with all possible combinations of (i) transition depth between the upper loose sediment layer and bottom compact layer at 0.20, 0.40, 0.60, 0.80 and 1 m depth and (ii) 1, 2, 3, 4 and 5 creeks over the 50-m cross-section.

Close to the creeks, we see a large significant effect ($p < 0.001$) of the transition depth on the spring tide drainage depth as well as on the neap tide drainage depth (Fig. 7a). However, as the transition of the soil layers gets deeper, the effect decreases. At 1 m from the creek edge, the number of creeks in the domain does not significantly alter the spring tide drainage depth ($p = 0.18$). The neap tide drainage depth, however, is significantly affected by the number of creeks ($p = 0.01$) . Until a transition depth of 60 cm, the drainage depth increases with the number of creeks. For transition depths larger than 80 cm, however, the drainage depth decreases when the number of creeks becomes larger than 3 (Fig. 7c). This effect can be attributed to the reduction in creek depth with an increasing number of creeks, as we applied a constant total creek cross-sectional area (see methods for reasoning). Further away from the creeks, the spring tide drainage depth is significantly affected by both the soil layer transition depth and the number of creeks ($p < 0.001$). Here also, at deeper soil layer transition depths, over 5 creeks in the domain do not increase the drainage depth anymore. Over the entire marsh domain, both the number of creeks and the soil layer transition depth affect the depth of the variably saturated zone, whereas closer to the creek the soil layer transition has a more profound effect.

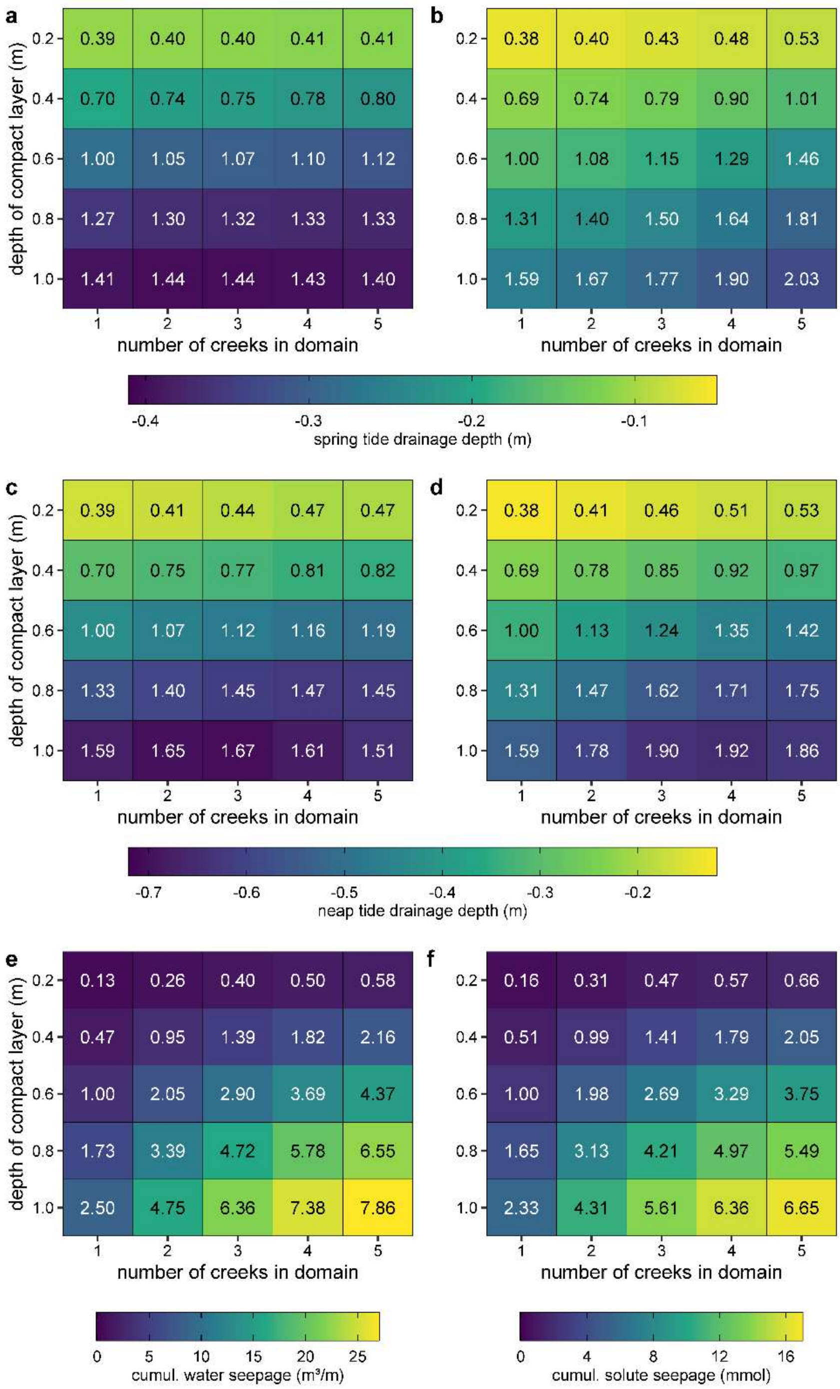

Fig. 7: a,b: spring tide drainage depth relative to the soil surface at 1 m and 4 m from the creek edge, respectively; b,c: neap tide drainage depth relative to the soil surface at 1 m and 4 m from the creek, respectively; e: cumulative water seepage volume after two spring tide – neap tide cycles (expressed in volume per meter creek length); f: cumulative solute seepage after two spring tide – neap tide cycles. Labels in the plots represent the value of the respective scenario relative to the base scenario (with 1 creek in the domain and transition depth at 0.60 m below the soil surface).

Both the number of creeks in the domain and the soil layer transition depth positively affect the volume of water that effectively flows through the marsh soil over a given timespan (Fig. 7e). Compared to the base scenario, multiplying the number of creeks with a factor of 2, leads to more than a doubling of the cumulative water seepage flux. The effects on the cumulative solute flux are similar (Fig. 7f), although, as mentioned earlier, the cumulative solute flux on a longer time span is expected to congregate for the different scenarios, as it is ultimately limited by depletion of solute in the domain.

The proportion of the time that the soil is saturated (the soil saturation index, SSI) is affected by both the number of creeks in the domain and the depth of the soil transition. Here, we assume that a specific location in the soil is unsaturated when the local soil moisture content is 1% lower than the soil moisture content at saturation. We compare the extent of the zone where the SSI is under 95% between the different scenarios.

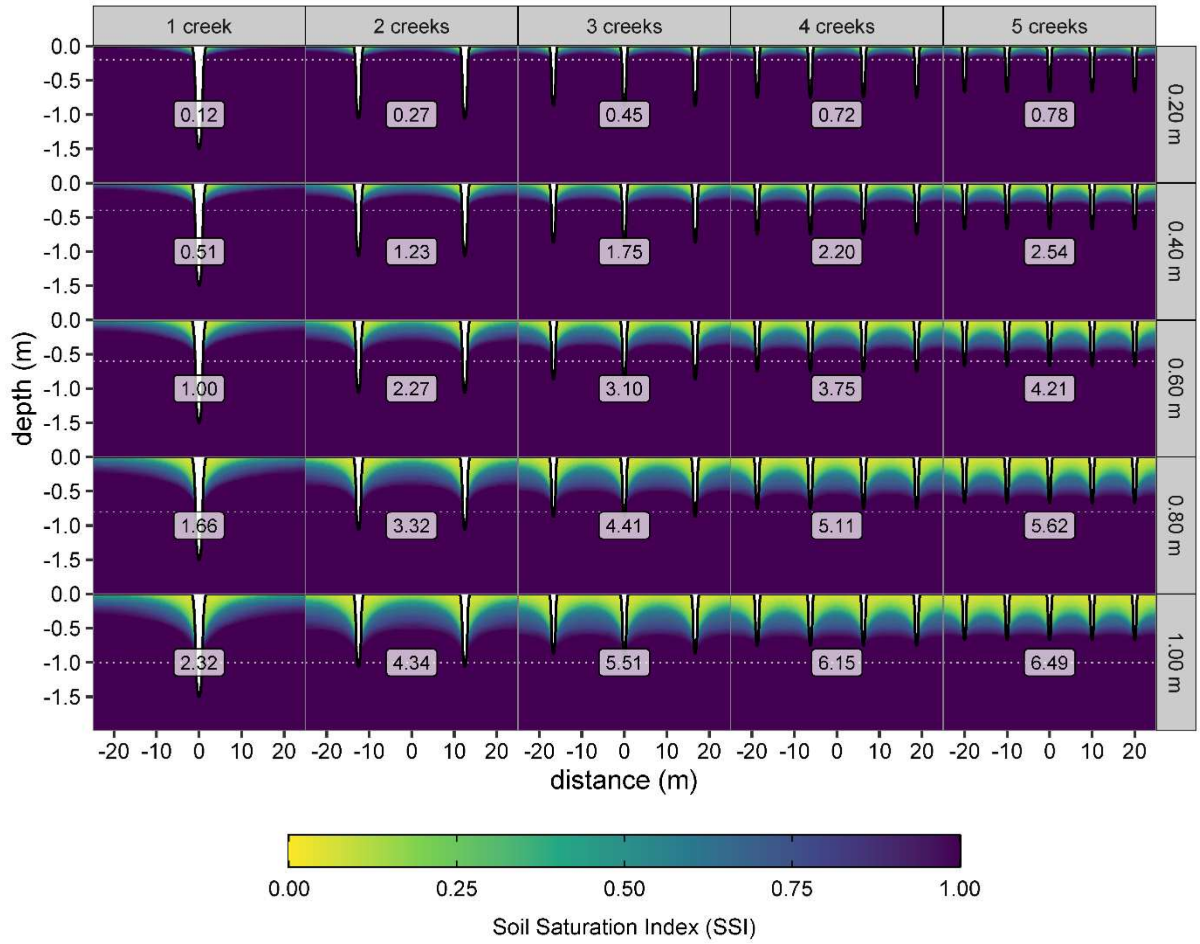

Fig. 8: Spatial distribution of the Soil Saturation Index for all the scenarios during two spring tide – neap tide cycles. An SSI of 1 means that the soil is always saturated. Saturated soil is defined as soil where $\theta \geq \theta_s - 0.01$. The labels indicate the proportion of the domain that is unsaturated for at least 50% of the simulated timespan, relative to the reference scenario (with 1 creek and transition depth at 0.60 m), where this proportion is 0.025. Dashed horizontal lines indicate the soil layer transition.

Both the number of creeks in the domain and the soil layer transition depth affect the SSI. In all scenarios, the extent of the variably saturated zone is limited to the layer of newly deposited/amended soil. A larger number of creeks increases the extent of the variably saturated zone (fig 8). Although the marsh platform is inundated for 17% of the time, the SSI near the surface is lower than this value. This indicates that the soil can remain (slightly) unsaturated, even during inundation.

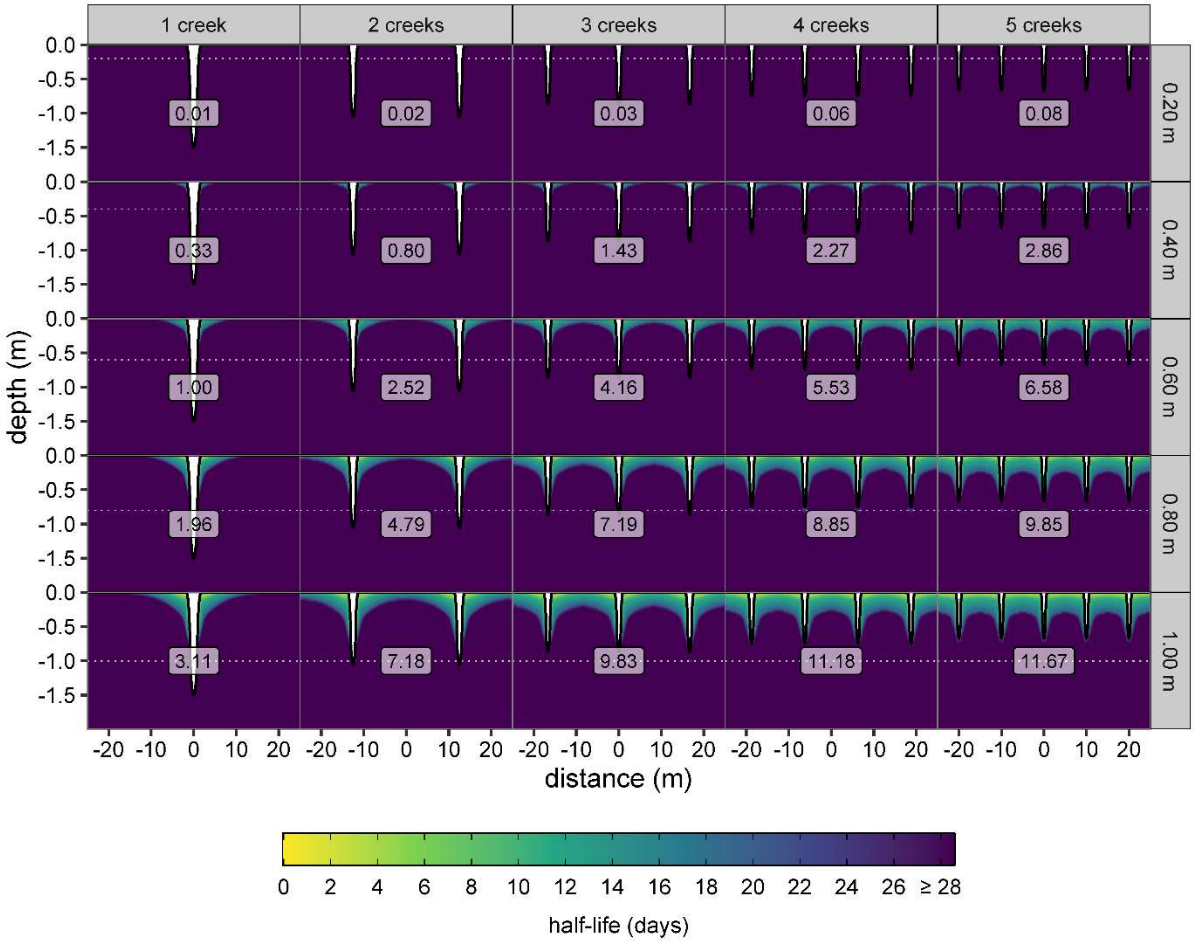

Fig. 9: spatial distribution of the time it takes to remove half of the solute mass (half-life) for all the scenarios. Half-lives of over 28 days indicate that the solute mass remained larger than 50% of the initial mass during the entire simulation time (two spring tide-neap tide cycles). Labels indicate the proportion of the domain in which at least 50% of the solute mass was removed within the simulation time, relative to the base scenario (1 creek and transition depth at 0.60 m), in which this proportion is 0.017. The dotted white lines indicate the transition between the soil layers.

We further investigated the removal of a conservative tracer in the domain in which the porewater has an initial concentration of 1 and the concentration in the flooding water is 0. We calculated for every node in the domain the time it takes to remove half of the solute mass in that node. Close to the creek edges, this ‘half-life’ time is short, as the solute is transported by advection to the creek during the falling tide and the porewater is replaced by infiltrating surface water during the rising tide (Fig. 9). The concentration near the creek edges increases again when porewater from the marsh interior flows towards the creeks during the next falling tide. Hence, the concentration near the creek edges follows an oscillating pattern (not shown).

In the marsh interior, where the soil is mostly saturated, solute is predominantly removed by diffusive processes. Initially, the tracer is rapidly removed but the removal rate declines as the most active zone gets depleted in tracer mass. We can expect that in the compact soil in the marsh interior, it can take decades to centuries for all the solute tracer to be removed from the porewater.

4. DISCUSSION

Agricultural soil compaction alters the structure of the soil in formerly embanked and drained wetlands. When tidal marshes are restored on such compact agricultural land, their subsurface hydrology is impaired compared to natural tidal marshes, which may result in reduced vegetation growth and altered biogeochemical cycling. The compact agricultural soil layer typically persists long after restoration and forms a barrier for groundwater dynamics and associated ecosystem functioning (Crooks and Pye, 2000; Tempest et al., 2015; Van Putte et al., 2020). Regarding the latter, there is a critical need for understanding of subsurface ecohydrology in restored tidal marshes to optimize delivery of ecosystem services in future tidal marsh restoration projects. In this paper, we use a vertical 2D variably saturated dual porosity groundwater model to simulate groundwater flow in a restored tidal marsh with a compact subsoil. For the first time for tidal marshes, we also solve the solute transport problem using the advection dispersion equation. This enables us to calculate the residence time and half-life of a non-reactive tracer, which is not possible by solving only the flow problem. With this coupled model, we are able to accurately predict the pressure head distribution in the marsh up to 10 m from the creek edges. Our model results clearly show that the compact layer limits tidally induced porewater circulation in the marsh soil.

The model is focused on tidally induced groundwater dynamics and solute transport and does not consider porewater extraction by evapotranspiration by the vegetation and porewater recharge by precipitation. In this study, we only considered porewater circulation during winter, when the effects of evapotranspiration are negligible. Nevertheless, evapotranspiration has a major effect on porewater removal in the growth season, especially in the marsh interior where porewater drainage towards creeks is limited (Hemond and Fifield, 1982; Nuttle, 1988). We observed that during the growth season, neap tide drainage depths in the marsh interior are deeper compared to the winter season (data not shown). Near the creek, tidally induced porewater circulation prevails, also in the summer growing season. While our calculations therefore might overestimate the soil saturation index, especially for marsh interior locations farther away from creeks, we argue that seepage fluxes, residence times and associated effects on biogeochemical cycling are much more affected by tidally induced porewater circulation. After all, we showed, in accordance with Harvey et al. (1987) that the majority of the seepage and solute transport originates from the soil in the vicinity of tidal creeks. Our model also does not consider shrinking and swelling and compression of the soil matrix during tidal inundation. According to Wilson and Morris (2012) and Gardner and Wilson (2006), omitting soil compressibility effects from the model can result in overestimation of seepage fluxes. However, Xin et al. (2009b) point out that the effect of soil compressibility is minimal and can be ignored for soils with a hydraulic conductivity larger than 10^{-6} m/s, which is the case for the tidally deposited sediment in our model ($3.50 \cdot 10^{-5}$ m/s). Variably saturated pore water flow in our model is governed by the single phase (only water flow) form of the Richards' equation (Richards, 1931) and therefore does not explicitly consider the flow of air in soil pores, which can have a significant effect on the estimation of soil aeration. Not incorporating the entrapment of air may lead to a persistent unsaturated zone and an overestimation of infiltration volumes during inundation (Li et al., 2005). However, Xin et al. (2009b) argue that it is unlikely that such a persistent unsaturated zone would exist in the presence of large macropores (e.g. crab burrows) as is the case in the restored tidal marsh considered in our study.

Decomposition of large organic matter parts (e.g. plant stems and roots) leads to void spaces that act as preferential flow channels and, in this way, further enhances porewater circulation in the marsh soil. Previous studies have shown that groundwater flow in tidal marshes is often dominated by preferential flow through macropores (Van Putte et al., 2020; Xin et al., 2009b; Xin et al., 2016). Therefore, we constructed a model domain consisting of a micropore region and a macropore region that can exchange porewater based on the respective volumetric soil moisture content in both regions. In this way, we accounted for the fast initial drainage trough the macropores and a slower drainage during neap tides when water from the micropore region is transferred to the macropore region and drains towards the creeks (Fig. 4). In general, our model was able to simulate the pressure head distribution with good accuracy up to 10 m from the creek edge. Further away from the creek edge, our model systematically overestimated the groundwater level compared to field measurements. We hypothesize that this is due to the choice of boundary conditions. To generalize our model results, we applied a flat surface topography to our model, whereas in the field the marsh elevation decreases further away from the creek (Fig. 1c), increasing the hydraulic gradient. Furthermore, our model considers only groundwater flow along a one-dimensional transect and in relation to one creek. The farther away from that one considered creek, the larger the chance that the observed groundwater dynamics are related to more complex flow patterns. This may also contribute to the increasing deviation of model simulations and observations with increasing distance from the considered creek. In our simulations we did not consider evapotranspiration, soil compressibility and air entrapment. As a result, our model has fewer input parameters and is therefore easier to apply and modify by other scientists aiming to support stakeholders in decision making concerning optimal marsh restoration design.

Based on scenario analyses, we identify and evaluate design measures for marsh restoration, which can alleviate the effects of the compact layer on the hindered groundwater circulation.

Even a decade after the marsh restoration, the compact soil layer forms a barrier for soil-groundwater interactions. Our model results suggest that approximately 6 times more water would pass through the marsh soil during a spring tide – neap cycle in the absence of the compact layer, compared to the present situation (Fig. 4). The median hydraulic conductivity in the compact layer in our study area is $4.16 \cdot 10^{-8}$ m/s, and is therefore classified as nearly impermeable following the classification of Bear (1972). The presence of the compact layer decreases the drainage depth and increases the soil saturation index in tidal marshes, leading to more frequent waterlogged soils and reduced aeration depth (Fig.6a). This soil aeration is, however, crucial for the establishment and zonation of tidal wetland plants; waterlogged soils can inhibit the growth of several plant species (Hou et al., 2020). The soil saturation index of the upper marsh soil correlates with spatial plant zonation in tidal wetlands (Ursino et al., 2004; Xin et al., 2013). Tidal marsh habitats adjacent to tidal creeks are less prone to vegetation die-off and provide better plant growth conditions. The absence of a developed creek network may therefore lead to the formation of pools and waterlogged soils (Schepers et al., 2017). Thus, an extended creek network is beneficial for both surface and subsurface drainage.

Tidal marshes restored on formerly embanked agricultural land often exhibit a lower creek density compared to natural tidal marshes. The presence of the compact agricultural soil inhibits or slows down natural creek incision and creek network development (Liu et al., 2020; Vandenbruwaene et al., 2012). Hence initial excavation of creeks may be advised to stimulate porewater seepage and soil aeration. We found that compared to the reference situation (1 creek in a 50 m transect and the compact layer at a depth of 60 cm), doubling the creek density more than doubles the proportion of the marsh soil with an SSI smaller than 50 % (Fig. 8) and the volume of water that flows through the marsh soil. However, as more creeks are added to the domain, their depth decreases to conserve the total creek cross sectional area. As a consequence, the effect of excavating more creeks on groundwater flow decreases with an increasing number of creeks already present. A creek density of more than 3 creeks in 50 m even reduces the drainage depth (Fig. 7c), highlighting the effect of creek depth on drainage depths. When the compact layer is shallow (i.e. in the early stage after the restoration), however, the reduction in drainage depth with an increasing creek density was not observed. We conclude that especially the interaction between the creek density and the depth of the soil transition determines soil aeration, drainage depths and seepage fluxes. Soil amendments (by tilling the soil and/or mixing it with organic matter) increase the hydraulic conductivity of the soil (Kuncoro et al., 2014) and increase the depth from the soil surface to the compact layer. Based on the results of the scenario analyses, we can state that increasing the depth to the compact layer promotes soil aeration, seepage fluxes and soil-groundwater interactions, which are crucial for biogeochemical cycling in tidal marshes. A combination of both creek excavation and soil amendments is therefore suggested for new tidal marsh restoration projects.

Porewater drainage is the main driver for silica recycling in tidal marshes, which plays a major role in estuarine primary production by diatoms (Struyf et al., 2005). Dissolved silica, resulting from the dissolution of biogenic silica from marsh vegetation, for example, is advectively transported with the porewater draining towards the creeks (Struyf et al., 2006). Our model simulations indicate that the residence time of the porewater in the marsh soil decreases when soil amendments and/or creek excavation are applied (Fig. 7c,d). In the compact subsoil, the half-life of the solute tracer exceeds the simulation time (28 days). This suggests that dissolved nutrients in the compact layer reside months or even years before seeping out of the creek banks, which is consistent with Xin et al. (2011). As the availability of biogenic silica (BSi) in most tidal marshes is constantly high and dissolution occurs fast (Struyf et al., 2007), we expect an increased delivery of dissolved silica (DSi) to the estuary when residence times are shorter. With a shallow compact layer and high residence times, further dissolution of BSi might be hampered due to high concentrations of DSi already present in the porewater. According to our model results, silica delivery could be enhanced by ensuring a sufficient creek density and an upper porous soil layer. Both the number of creeks in the domain and the depth to the compact layer affect the residence time and turnover rate of nutrients in the marsh porewater.

Increased soil aeration by creek excavation and soil amendments is expected to increase nitrification processes as those processes are aerobic, and subsequent denitrification which is primarily limited by the availability of nitrate and the presence of organic carbon (Martin and Reddy, 1997; Wolf et al., 2011). Soil amendments in which organic matter is added can thus promote denitrification. On the other hand, faster drainage and increased soil aeration facilitates organic matter mineralization and can therefore decrease the contribution of the marsh to carbon sequestration (e.g. Guimond et al., 2020), although further research is needed to investigate the impact of soil aeration on carbon sequestration in restored tidal marshes.

Excavating a denser creek network does not only alter subsurface flow, soil aeration and nutrient cycling, but will also affect surface flow hydrodynamics and sedimentation – erosion processes, and as such influence the bio-geomorphic development of the restored marsh (Gourgue et al., 2021). Although this is beyond the scope of this paper, it is clear that marsh design options can have different effects on the various functions and ecosystem services of restored marshes. With this paper, we contribute to the knowledge on the effect of different design options on ecosystem functioning, so that stakeholders of a marsh restoration project can make a design based on prioritizing the delivery of certain ecosystem services.

5. CONCLUSIONS

- Using a dual porosity groundwater model, we were able to accurately simulate pressure head dynamics in a restored tidal marsh up to 10 m from the creek edge, indicating the importance of macropore flow in tidal marsh soils.
- The compact agricultural subsoil is 1476 times less permeable compared to the overlying layer of tidally deposited sediment and therefore forms a barrier for groundwater – soil interactions
- According to our model simulations, 6.06 times less water passes through the marsh soil and 5.84 times less solute was removed in the reference situation compared to a scenario in which the compact subsoil is absent
- A scenario analyses revealed that doubling the creek density or increasing the depth to the compact layer by 20 cm both more than doubles the volume of groundwater processed by the marsh soil.
- Initial creek initiation and soil amendments are therefore recommended to improve groundwater – soil interactions in newly restored tidal marshes.
- While increased seepage flows are expected to be beneficial for some ecosystem services such as the delivery of DSi to the estuary and removal of nitrogen from the surface water, other ecosystem services such as carbon sequestration might be negatively affected by increased soil aeration.

6. ACKNOWLEDGEMENTS

Niels Van Putte is SB PhD fellow at FWO (Research Foundation Flanders) project no. 1S17517N. The authors are grateful to Dimitri Van Pelt for field assistance and to Maarten Volckaert for help with the analyses of soil hydraulic properties.

7. ONLINE APPENDIX

7.1. Sensitivity analyses

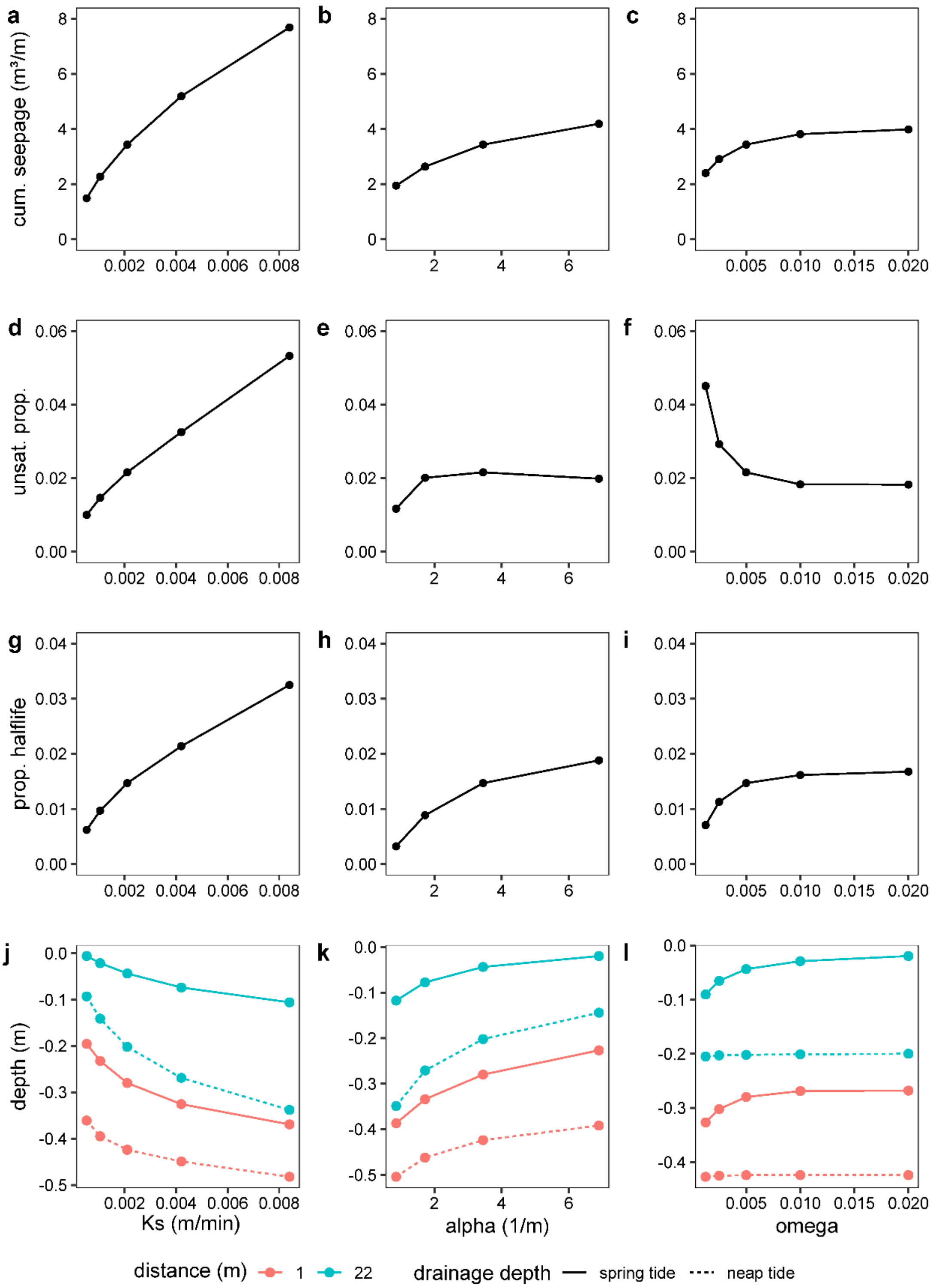

Fig. 10: Sensitivity to the hydraulic conductivity (K_s) (a,d,g,j), the α value (b,e,h,k), the mass transfer coefficient (ω) (c,f,i,l) of (a,b,c) the cumulative seepage flux, (d,e,f) the proportion of the domain in which the soil moisture content drops below 0.5 during the modeled time span, (g,h,i) the proportion of the domain in which at least 50 % of the solute mass is removed during the modeled timespan, (j,k,l) the spring tide drainage depth (solid line) and neap tide drainage depth (dashed line) in the near creek zone (red line) and the marsh interior (blue line)

The hydraulic conductivity (K_s) has the most profound effect on all simulated variables (Fig. 10 a,d,j,g). In the field study, we found that K_s ranges several orders of magnitude in the newly deposited sediment (Fig. 3). A good estimate of the saturated hydraulic conductivity is therefore essential to accurately simulate the subsurface hydrology. In our study, we calibrated the K_s to obtain the best ME values for the pressure heads. The K_s value that lead to the best simulated pressure heads (3.50·10-5 m/s) was well within the range of the field measured K_s values (Fig. 3).

The α value is positively correlated with the cumulative seepage flux, but negatively correlated with the drainage depth (fig. 10 b,k). The α value is inversely related to the air entry value (the minimum applied suction at which the soil starts to desaturate). Therefore, a smaller α value indicates a higher air entry value, which means that a higher suction needs to be applied for a similar volume of drainage. Hence the deeper groundwater drainage levels at a lower α value.

The model performance increased when switching to a dual porosity model based on water mass transfer (EQ 6). As the water mass transfer coefficient (ω) was unknown, we ran several model simulations with different ω values to calibrate the model. Model runs with a smaller ω value (i.e. less transfer between the mobile and immobile regions) show a faster initial drainage compared to model runs with a higher ω value (i.e. more transfer between the two regions). As a result, the spring tide drainage depth increases with a decreasing ω value. During neap tide drainage, the final drainage depth is not affected by the ω value, as the fast initial drainage slows down when the groundwater level approximates the compact soil layer. A larger ω value leads to higher seepage fluxes and a faster solute exchange (Fig. 10 c,i).

8. REFERENCES

Bear, J., 1972. Dynamics of Fluids in Porous Media. American Elsevier Publishing Company.

Burden, A., Garbutt, R.A., Evans, C.D., Jones, D.L., Cooper, D.M., 2013. Carbon sequestration and biogeochemical cycling in a saltmarsh Subject to coastal managed realignment. Estuar Coast Shelf S 120, 12-20. doi: 10.1016/j.ecss.2013.01.014

Callaway, J.C., Zedler, J.B., Ross, D.L., 1997. Using tidal salt marsh mesocosms to aid wetland restoration. Restor Ecol 5, 135-146. doi: DOI 10.1046/j.1526-100X.1997.09716.x

Cao, M., Xin, P., Jin, G.Q., Li, L., 2012. A field study on groundwater dynamics in a salt marsh - Chongming Dongtan wetland. Ecol Eng 40, 61-69. doi: 10.1016/j.ecoleng.2011.12.018

Chapman, V.J., 1938. Studies in Salt-Marsh Ecology Sections I to III. Journal of Ecology 26, 144-179. doi: 10.2307/2256416

Chassagne, R.L., Lecroart, P., Beaugendre, H., Capo, S., Parisot, J.P., Anschutz, P., 2012. Silicic acid flux to the ocean from tidal permeable sediments: A modeling study. Comput Geosci-Uk 43, 52-62. doi: 10.1016/j.cageo.2012.02.014

Chirol, C., Haigh, I.D., Pontee, N., Thompson, C.E., Gallop, S.L., 2018. Parametrizing tidal creek morphology in mature saltmarshes using semi-automated extraction from lidar. Remote Sens Environ 209, 291-311. doi: https://doi.org/10.1016/j.rse.2017.11.012

Cox, T.J.S., 2017. Tides R-package v2.0: Muddy One. doi: 10.5281/zenodo.897843

Craft, C., Broome, S., Campbell, C., 2002. Fifteen years of vegetation and soil development after brackish-water marsh creation. Restor Ecol 10, 248-258. doi: DOI 10.1046/j.1526-100X.2002.01020.x

Cresswell, H.P., Green, T.W., McKenzie, N.J., 2008. The Adequacy of Pressure Plate Apparatus for Determining Soil Water Retention. Soil Sci Soc Am J 72, 41-49. doi: https://doi.org/10.2136/sssaj2006.0182

Crooks, S., Pye, K., 2000. Sedimentological controls on the erosion and morphology of saltmarshes: implications for flood defence and habitat recreation. Geol Soc Spec Publ 175, 207-222. doi: 10.1144/Gsl.Sp.2000.175.01.16

D'Alpaos, A., Lanzoni, S., Marani, M., Rinaldo, A., 2010. On the tidal prism - channel area relations. J Geophys Res-Earth 115. doi: Artn F01003

10.1029/2008jf001243

Darcy, H., 1856. Les fontaines publiques de la ville de Dijon: exposition et application. Victor Dalmont.

Eijkelkamp Agrisearch Equipments, 2013. laboratory-Permeameters: Operation instructions, Giesbeek, The Netherlands.

Eijkelkamp Soil & Water, 2019. Sandbox for pF-determination: User manual, Giesbeek, The Netherlands.

Fei, Y.H., She, D.L., Gao, L., Xin, P., 2019. Micro-CT assessment on the soil structure and hydraulic characteristics of saline/sodic soils subjected to short-term amendment. Soil Till Res 193, 59-70. doi: 10.1016/j.still.2019.05.024

Gardner, L.R., 2005a. A modeling study of the dynamics of pore water seepage from intertidal marsh sediments. Estuar Coast Shelf S 62, 691-698. doi: 10.1016/j.ecss.2004.10.005

Gardner, L.R., 2005b. Role of geomorphic and hydraulic parameters in governing pore water seepage from salt marsh sediments. Water Resour Res 41. doi: 10.1029/2004wr003671

Gardner, L.R., 2007. Role of stratigraphy in governing pore water seepage from salt marsh sediments. Water Resour Res 43. doi: Artn W07505

10.1029/2006wr005338

Gardner, L.R., Wilson, A.M., 2006. Comparison of four numerical models for simulating seepage from salt marsh sediments. Estuar Coast Shelf S 69, 427-437. doi: 10.1016/j.ecss.2006.05.009

Gerke, H.H., van Genuchten, M.T., 1993. Evaluation of a 1st-Order Water Transfer Term for Variably Saturated Dual-Porosity Flow Models. Water Resour Res 29, 1225-1238. doi: Doi 10.1029/92wr02467

Gibson, K.D., Zedler, J.B., Langis, R., 1994. Limited Response of Cordgrass (Spartina-Foliosa) to Soil Amendments in a Constructed Marsh. Ecol Appl 4, 757-767. doi: Doi 10.2307/1942006

Goode, D.J., 1996. Direct Simulation of Groundwater Age. Water Resour Res 32, 289-296. doi: 10.1029/95wr03401

Gourgue, O., van Belzen, J., Schwarz, C., Vandenbruwaene, W., Vanlede, J., Belliard, J.P., Fagherazzi, S., Bouma, T.J., van de Koppel, J., Temmerman, S., 2021. Biogeomorphic modeling to assess resilience of tidal marsh restoration to sea level rise and sediment supply. Earth Surf. Dynam. Discuss. 2021, 1-38. doi: 10.5194/esurf-2021-66

Guimond, J.A., Yu, X., Seyfferth, A.L., Michael, H.A., 2020. Using Hydrological-Biogeochemical Linkages to Elucidate Carbon Dynamics in Coastal Marshes Subject to Relative Sea Level Rise. Water Resour Res 56, e2019WR026302. doi: https://doi.org/10.1029/2019WR026302

Harvey, J.W., Germann, P.F., Odum, W.E., 1987. Geomorphological Control of Subsurface Hydrology in the Creek-Bank Zone of Tidal Marshes. Estuar Coast Shelf S 25, 677-691. doi: 10.1016/0272-7714(87)90015-1

Harvey, J.W., Nuttle, W.K., 1995. Fluxes of Water and Solute in a Coastal Wetland Sediment .2. Effect of Macropores on Solute Exchange with Surface-Water. J Hydrol 164, 109-125. doi: Doi 10.1016/0022-1694(94)02562-P

Havens, K.J., Varnell, L.M., Watts, B.D., 2002. Maturation of a constructed tidal marsh relative to two natural reference tidal marshes over 12 years. Ecol Eng 18, 305-315. doi: Doi 10.1016/S0925-8574(01)00089-1

Hemond, H.F., Fifield, J.L., 1982. Subsurface Flow in Salt-Marsh Peat - a Model and Field-Study. Limnol Oceanogr 27, 126-136. doi: 10.4319/lo.1982.27.1.0126

Holz, M., Heil, S.R., Sacco, A., 2000. Temperature-dependent self-diffusion coefficients of water and six selected molecular liquids for calibration in accurate H-1 NMR PFG measurements. Physical Chemistry Chemical Physics 2, 4740-4742. doi: DOI 10.1039/b005319h

Hou, W., Zhang, R., Xi, Y., Liang, S., Sun, Z., 2020. The role of waterlogging stress on the distribution of salt marsh plants in the Liao River estuary wetland. Global Ecology and Conservation 23, e01100. doi: https://doi.org/10.1016/j.gecco.2020.e01100

Hughes, C.E., Binning, P., Willgoose, G.R., 1998. Characterisation of the hydrology of an estuarine wetland. J Hydrol 211, 34-49. doi: 10.1016/S0022-1694(98)00194-2

Jacobs, S., Beauchard, O., Struyf, E., Cox, T.J.S., Maris, T., Meire, P., 2009. Restoration of tidal freshwater vegetation using controlled reduced tide (CRT) along the Schelde Estuary (Belgium). Estuar Coast Shelf S 85, 368-376. doi: 10.1016/j.ecss.2009.09.004

Jaynes, D.B., Horton, R., 1998. Field parameterization of the mobile/immobile domain model., in: Selim, H.M., Ma, L. (Eds.), Physical Nonequilibrium in Soils: Modeling and Application. Ann Arbor Press, Chelsea, MI, pp. 297-310.

Kadiri, M., Spencer, K.L., Heppell, C.M., Fletcher, P., 2011. Sediment characteristics of a restored saltmarsh and mudflat in a managed realignment scheme in Southeast England. Hydrobiologia 672, 79-89. doi: 10.1007/s10750-011-0755-8

Kuncoro, P.H., Koga, K., Satta, N., Muto, Y., 2014. A study on the effect of compaction on transport properties of soil gas and water I: Relative gas diffusivity, air permeability, and saturated hydraulic conductivity. Soil and Tillage Research 143, 172-179. doi: https://doi.org/10.1016/j.still.2014.02.006

Lawrence, D.S.L., Allen, J.R.L., Havelock, G.M., 2004. Salt Marsh Morphodynamics: An Investigation of Tidal Flows and Marsh Channel Equilibrium. J Coastal Res 20, 301-316. doi:

Li, H.L., Li, L., Lockington, D., 2005. Aeration for plant root respiration in a tidal marsh. Water Resour Res 41. doi: Artn W06023

10.1029/2004wr003759

Liu, Z., Fagherazzi, S., She, X., Ma, X., Xie, C., Cui, B., 2020. Efficient tidal channel networks alleviate the drought-induced die-off of salt marshes: Implications for coastal restoration and management. Sci Total Environ 749, 141493. doi: https://doi.org/10.1016/j.scitotenv.2020.141493

Maris, T., Cox, T.J.S., Temmerman, S., De Vleeschauwer, P., Van Damme, S., De Mulder, T., Van den Bergh, E., Meire, P., 2007. Tuning the tide: creating ecological conditions for tidal marsh development in a flood control area. Hydrobiologia 588, 31-43. doi: 10.1007/s10750-007-0650-5

Marois, D.E., Stecher, H.A., 2020. A simple, dynamic, hydrological model for mesotidal salt marshes. Estuar Coast Shelf S 233. doi: ARTN 106486

10.1016/j.ecss.2019.106486

Martin, J.F., Reddy, K.R., 1997. Interaction and spatial distribution of wetland nitrogen processes. Ecol Model 105, 1-21. doi: https://doi.org/10.1016/S0304-3800(97)00122-1

Millington, R., Quirk, J.P., 1961. Permeability of Porous Solids. T Faraday Soc 57, 1200-&. doi: DOI 10.1039/tf9615701200

Moffett, K.B., Gorelick, S.M., McLaren, R.G., Sudicky, E.A., 2012. Salt marsh ecohydrological zonation due to heterogeneous vegetation–groundwater–surface water interactions. Water Resour Res 48. doi: 10.1029/2011WR010874

Mualem, Y., 1976. A new model for predicting the hydraulic conductivity of unsaturated porous media. Water Resour Res 12, 513-522. doi: 10.1029/WR012i003p00513

Nash, J.E., Sutcliffe, J.V., 1970. River flow forecasting through conceptual models part I — A discussion of principles. J Hydrol 10, 282-290. doi: https://doi.org/10.1016/0022-1694(70)90255-6

Nuttle, W.K., 1988. The Extent of Lateral Water-Movement in the Sediments of a New England Salt-Marsh. Water Resour Res 24, 2077-2085. doi: 10.1029/WR024i012p02077

O'Brien, E.L., Zedler, J.B., 2006. Accelerating the restoration of vegetation in a southern California salt marsh. Wetl Ecol Manag 14, 269-286. doi:

Oosterlee, L., Cox, T.J.S., Vandenbruwaene, W., Maris, T., Temmerman, S., Meire, P., 2017. Tidal Marsh Restoration Design Affects Feedbacks Between Inundation and Elevation Change. Estuar Coast. doi: 10.1007/s12237-017-0314-2

Ott, E.T., Galbraith, J.M., Daniels, W.L., Aust, W.M., 2020. Effects of amendments and microtopography on created tidal freshwater wetland soil morphology and carbon. Soil Sci Soc Am J 84, 638-652. doi: 10.1002/saj2.20057

Richards, L.A., 1931. Capillary conduction of liquids through porous mediums. J Appl Phys 1, 318-333. doi:

Schepers, L., Kirwan, M., Guntenspergen, G., Temmerman, S., 2017. Spatio-temporal development of vegetation die-off in a submerging coastal marsh. Limnol Oceanogr 62, 137-150. doi: 10.1002/lno.10381

Scott, B., Baldwin, A., Ballantine, K., Palmer, M., Yarwood, S., 2020. The role of organic amendments in wetland restorations: Organic Amendments Wetland Restoration. Restor Ecol. doi: 10.1111/rec.13179

Senja, M., Simunek, J., van Genuchten, M.T., 2017. HYDRUS 2D/3D, version 2.05.0240 ed. PC-Progress s.r.o., Prague, Czech Republic.

Simunek, J., Jarvis, N.J., van Genuchten, M.T., Gardenas, A., 2003. Review and comparison of models for describing non-equilibrium and preferential flow and transport in the vadose zone. J Hydrol 272, 14-35. doi:

Spencer, K.L., Carr, S.J., Diggens, L.M., Tempest, J.A., Morris, M.A., Harvey, G.L., 2017. The impact of pre-restoration land-use and disturbance on sediment structure, hydrology and the sediment geochemical environment in restored saltmarshes. Sci Total Environ 587, 47-58. doi: 10.1016/j.scitotenv.2016.11.032

Struyf, E., Dausse, A., Van Damme, S., Bal, K., Gribsholt, B., Boschker, H.T.S., Middelburg, J.J., Meire, P., 2006. Tidal marshes and biogenic silica recycling at the land-sea interface. Limnol Oceanogr 51, 838-846. doi:

Struyf, E., Van Damme, S., Gribsholt, B., Bal, K., Beauchard, O., Middelburg, J.J., Meire, P., 2007. Phragmites australis and silica cycling in tidal wetlands. Aquat Bot 87, 134-140. doi: 10.1016/j.aquabot.2007.05.002

Struyf, E., Van Damme, S., Gribsholt, B., Middelburg, J.J., Meire, P., 2005. Biogenic silica in tidal freshwater marsh sediments and vegetation (Schelde estuary, Belgium). Mar Ecol Prog Ser 303, 51-60. doi: DOI 10.3354/meps303051

Suckow, A., 2014. The age of groundwater – Definitions, models and why we do not need this term. Applied Geochemistry 50, 222-230. doi: https://doi.org/10.1016/j.apgeochem.2014.04.016

Tempest, J.A., Harvey, G.L., Spencer, K.L., 2015. Modified sediments and subsurface hydrology in natural and recreated salt marshes and implications for delivery of ecosystem services. Hydrol Process 29, 2346-2357. doi: 10.1002/hyp.10368

Tovey, E.L., Pontee, N.I., Harvey, R., 2009. Managed Realignment at Hesketh Out Marsh West. Proceedings of the Institution of Civil Engineers - Engineering Sustainability 162, 223-228. doi: 10.1680/ensu.2009.162.4.223

Turnadge, C., Smerdon, B.D., 2014. A review of methods for modelling environmental tracers in groundwater: Advantages of tracer concentration simulation. J Hydrol 519, 3674-3689. doi: 10.1016/j.jhydrol.2014.10.056

Ursino, N., Silvestri, S., Marani, M., 2004. Subsurface flow and vegetation patterns in tidal environments. Water Resour Res 40. doi: 10.1029/2003wr002702

Van Genuchten, M., Leij, F., Yates, S., Williams, J., 1991. The RETC Code for Quantifying Hydraulic Functions of Unsaturated Soils. EPA/600/2-91/065, R.S. 83. doi:

van Genuchten, M.T., 1980. A Closed-form Equation for Predicting the Hydraulic Conductivity of Unsaturated Soils. Soil Sci Soc Am J 44, 892-898. doi: 10.2136/sssaj1980.03615995004400050002x

van Genuchten, M.T., Wierenga, P.J., 1976. Mass-Transfer Studies in Sorbing Porous-Media .1. Analytical Solutions. Soil Sci Soc Am J 40, 473-480. doi: DOI 10.2136/sssaj1976.03615995004000040011x

Van Putte, N., Temmerman, S., Verreydt, G., Seuntjens, P., Maris, T., Heyndrickx, M., Boone, M., Joris, I., Meire, P., 2020. Groundwater dynamics in a restored tidal marsh are limited by historical soil compaction. Estuarine, Coastal and Shelf Science 244, 106101. doi: https://doi.org/10.1016/j.ecss.2019.02.006

Vandenbruwaene, W., Bouma, T.J., Meire, P., Temmerman, S., 2013. Bio-geomorphic effects on tidal channel evolution: impact of vegetation establishment and tidal prism change. Earth Surf Proc Land 38, 122-132. doi: 10.1002/esp.3265

Vandenbruwaene, W., Meire, P., Temmerman, S., 2012. Formation and evolution of a tidal channel network within a constructed tidal marsh. Geomorphology 151, 114-125. doi: 10.1016/j.geomorph.2012.01.022

Vanlede, J., Maximova, T., Vandenbruwaene, W., Plancke, Y., Verwaest, T., Mostaert, F., 2015. Inrichtingsplan Hedwige-Prosperpolder: Deelrapport 2 – Resultaten van het hydrodynamisch model. Versie 6.0., Waterbouwkundig Laboratorium: Antwerpen, België.

Wang, W.W., Li, D.J., Zhou, J.L., Gao, L., 2011. Nutrient dynamics in pore water of tidal marshes near the Yangtze Estuary and Hangzhou Bay, China. Environ Earth Sci 63, 1067-1077. doi: 10.1007/s12665-010-0782-1

Wilson, A.M., Evans, T., Moore, W., Schutte, C.A., Joye, S.B., Hughes, A.H., Anderson, J.L., 2015. Groundwater controls ecological zonation of salt marsh macrophytes. Ecology 96, 840-849. doi: 10.1890/13-2183.1

Wilson, A.M., Gardner, L.R., 2006. Tidally driven groundwater flow and solute exchange in a marsh: Numerical simulations. Water Resour Res 42. doi: 10.1029/2005wr004302

Wilson, A.M., Morris, J.T., 2012. The influence of tidal forcing on groundwater flow and nutrient exchange in a salt marsh-dominated estuary. Biogeochemistry 108, 27-38. doi: 10.1007/s10533-010-9570-y

Wolf, E.C., Rejmankova, E., Cooper, D.J., 2019. Wood chip soil amendments in restored wetlands affect plant growth by reducing compaction and increasing dissolved phenolics. Restor Ecol 27, 1128-1136. doi: 10.1111/rec.12942

Wolf, K.L., Ahn, C., Noe, G.B., 2011. Development of Soil Properties and Nitrogen Cycling in Created Wetlands. Wetlands 31, 699-712. doi: 10.1007/s13157-011-0185-4

Wolters, M., Garbutt, A., Bakker, J.P., 2005. Salt-marsh restoration: evaluating the success of de-embankments in north-west Europe. Biological Conservation 123, 249-268. doi: 10.1016/j.biocon.2004.11.013

Xiao, K., Wilson, A.M., Li, H., Ryan, C., 2019. Crab burrows as preferential flow conduits for groundwater flow and transport in salt marshes: A modeling study. Adv Water Resour 132, 103408. doi: https://doi.org/10.1016/j.advwatres.2019.103408

Xie, H., Yi, Y., Hou, C., Yang, Z., 2020. In situ experiment on groundwater control of the ecological zonation of salt marsh macrophytes in an estuarine area. J Hydrol 585, 124844. doi: https://doi.org/10.1016/j.jhydrol.2020.124844

Xin, P., Gibbes, B., Li, L., Song, Z.Y., Lockington, D., 2010. Soil saturation index of salt marshes subjected to spring-neap tides: a new variable for describing marsh soil aeration condition. Hydrol Process 24, 2564-2577. doi: 10.1002/hyp.7670

Xin, P., Jin, G.Q., Li, L., 2009a. Modelling Study on Subsurface Flows Affected by Macro-Pores in Marsh Sediments. Advances in Water Resources and Hydraulic Engineering, Vols 1-6, 1394-1400. doi: Doi 10.1007/978-3-540-89465-0_244

Xin, P., Jin, G.Q., Li, L., Barry, D.A., 2009b. Effects of crab burrows on pore water flows in salt marshes. Adv Water Resour 32, 439-449. doi: 10.1016/j.advwatres.2008.12.008

Xin, P., Kong, J., Li, L., Barry, D.A., 2012. Effects of soil stratigraphy on pore-water flow in a creek-marsh system. J Hydrol 475, 175-187. doi: 10.1016/j.jhydrol.2012.09.047

Xin, P., Kong, J., Li, L., Barry, D.A., 2013. Modelling of groundwater-vegetation interactions in a tidal marsh. Adv Water Resour 57, 52-68. doi: 10.1016/j.advwatres.2013.04.005

Xin, P., Yu, X.Y., Lu, C.H., Li, L., 2016. Effects of macro-pores on water flow in coastal subsurface drainage systems. Adv Water Resour 87, 56-67. doi: 10.1016/j.advwatres.2015.11.007

Xin, P., Yuan, L.R., Li, L., Barry, D.A., 2011. Tidally driven multiscale pore water flow in a creek-marsh system. Water Resour Res 47. doi: 10.1029/2010wr010110

Xin, P., Zhou, T.Z., Lu, C.H., Shen, C.J., Zhang, C.M., D'Alpaos, A., Li, L., 2017. Combined effects of tides, evaporation and rainfall on the soil conditions in an intertidal creek-marsh system. Adv Water Resour 103, 1-15. doi: 10.1016/j.advwatres.2017.02.014

Xu, X., Xin, P., Zhou, T., Xiao, K., 2021. Effect of macropores on pore-water flow and soil conditions in salt marshes subject to evaporation and tides. Estuarine, Coastal and Shelf Science 261, 107558. doi: https://doi.org/10.1016/j.ecss.2021.107558

Zedler, J.B., 2000. Handbook for Restoring Tidal Wetlands. CRC Press.